


Changes in gene expression levels caused by H3K9me3/H3K9ac modifications are associated with BmCPV infection in *Bombyx mori*

Qunnan Qiu^{a,b,*}, Xinyu Tong^{a,*}, Min Zhu^{a,b,*}, Zhe Liu^a, Huilin Pang^a, Liuyang Li^a, Yongjie Feng^a, Xiaolong Hu^{a,b}, and Chengliang Gong ^{a,b}

^aSchool of Life Sciences, Soochow University, Suzhou, China; ^bAgricultural Biotechnology Research Institute, Agricultural Biotechnology and Ecological Research Institute, Soochow University, Suzhou, China

ABSTRACT

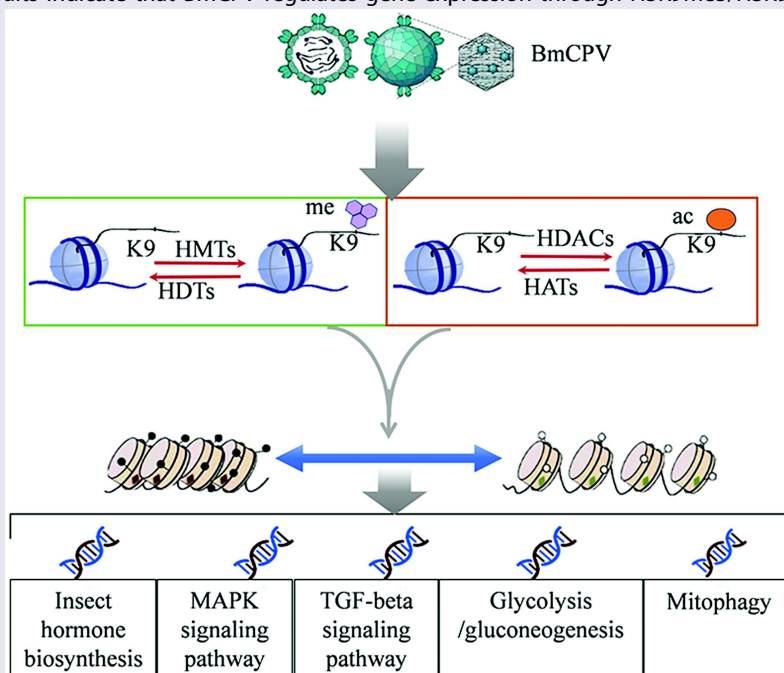
Changes in chromatin accessibility caused by histone modifications regulate gene transcription. However, little is known about associations between gene expression changes caused by histone modifications and viral infections. We investigate the midguts of silkworms infected with *Bombyx mori* cypovirus (BmCPV) at 48 h and 96 h post infection (CPV48 and CPV96), and corresponding midguts of uninfected silkworms (GUT48 and GUT96) using CUT&Tag-seq and RNA-seq. We report H3K9me3, H3K9ac, and gene expression profiles at the genome-wide level to change with BmCPV infection. Differential H3K9me3 peak-related genes were mainly enriched in MAPK, Wnt, and Hippo signalling pathways; Differential H3K9ac peaks-related genes were mainly enriched in the Hippo signalling, apoptosis, and citrate cycle pathways; and differentially expressed genes (DEGs) were mainly enriched in carbon metabolism, protein processing in endoplasmic reticulum, and glycolysis/gluconeogenesis pathways. Integration analysis between H3K9me3/H3K9ac peaks and gene expression revealed changes in gene expression profiles to be associated with alteration of H3K9me3/H3K9ac at promoters; gene expression correlates negatively with corresponding H3K9me3 signals in gene bodies, and positively with corresponding H3K9ac signals at the transcription start site. Intersection genes with \log_2 foldchange of both CUT&Tag-seq peak and RNA-seq FPKM > 1 were screened and annotated. Genes shared by differential H3K9me3 peak-related genes and DEGs were enriched in insect hormone biosynthesis, MAPK signalling, and TGF-beta signalling pathways, and genes shared by differential H3K9ac peak-related genes and DEGs were enriched in glycolysis/gluconeogenesis, TGF-beta signalling, and mitophagy pathways. These results indicate that BmCPV regulates gene expression through H3K9me3/H3K9ac.

ARTICLE HISTORY

Received 4 August 2024
Revised 2 May 2025
Accepted 19 May 2025


KEYWORDS

Bombyx mori; cypovirus; H3K9me3; H3K9ac; gene expression



CONTACT Xiaolong Hu  xlhu2013@suda.edu.cn; Chengliang Gong  gongcl@suda.edu.cn

*These authors contributed equally to this work.

 Supplemental data for this article can be accessed online at <https://doi.org/10.1080/21505594.2025.2510535>.

© 2025 The Author(s). Published by Informa UK Limited, trading as Taylor & Francis Group.

This is an Open Access article distributed under the terms of the Creative Commons Attribution-NonCommercial License (<http://creativecommons.org/licenses/by-nc/4.0/>), which permits unrestricted non-commercial use, distribution, and reproduction in any medium, provided the original work is properly cited. The terms on which this article has been published allow the posting of the Accepted Manuscript in a repository by the author(s) or with their consent.

Introduction

Histone modifications (including acetylation, methylation, phosphorylation, ubiquitylation, SUMOylation, ADP ribosylation, deimination, and proline isomerization) are common posttranslational modifications that are important in various intracellular physiological activities [1,2]. Of these, histone acetylation and histone methylation (especially histone lysine methylation) occur most commonly.

Histone lysine methylations have mainly occurred in lysine residues of histone 3 (H3) and histone 4 (H4) in the following forms: mono-, di-, and trimethylation [3]. Based on the effect on transcriptional activity, histone methylations have been classified into active and repressive histone marks. In eukaryotes, both euchromatin and heterochromatin are present [4]. Euchromatin with a loose structure is beneficial for the binding of transcription factors and gene expression, and heterochromatin, with a tightly intertwined structure, can repress the binding of transcription factors, leading to gene silence.

H3K9 methylations, especially H3K9 trimethylation (H3K9me3), are closely related to gene silencing and heterochromatin formation [5]. Endogenous retroviruses are silenced by the interaction of H3K9 methyltransferase SETDB1 with heterochromatin protein HP1 [6]. Virus proliferation is inhibited by H3K9 methylation, and H3K9 methyltransferase Suv39 h1-mediated H3K9me3 can induce inhibition of Epstein – Barr virus (EBV) *BZLF1* gene transcription in B95–8 cells, further repressing the transition of EBV-infected cells from latency to replicative cycles [7]. Both H3K9me3 and the trimethylation of lysine 27 of histone 3 (H3K27me3) increase with chromatin regulator CTCF knockdown, which repressed the lytic transcription of herpes simplex virus-1 [8,9]. Tripartite motif-containing protein 28 (Trim28) negatively inhibits prototype foamy virus (PFV) replication by acting as a transcriptional restriction factor that is enriched in viral long terminal repeat promoter and modulates the H3K9me3 mark [10]. EBV was also located in perichromatic regions that are enriched for acetylation of lysine 9 of histone 3 (H3K9ac) and trimethylation of lysine 4 of histone 3 (H3K4me3), which are associated with transcription activation. EBV nuclear antigen (EBNA) leader protein (LP) and EBNA2 preferentially interact with human B-cell transcription factors at or near pre-patterned promoter sites, further increasing activation-associated histone marks (such as H3K9ac) [11,12]. EBV oncoprotein EBNA3C can recruit histone activation epigenetic marks such as H3K4me1, H3K4me3, H3K9ac, and H3K27ac for transcriptional activation of autophagy genes [13].

Bovine herpesvirus 1 (BoHV-1) infection at the late stage can dramatically decrease histone H3 acetylation (H3K9ac and H3K18ac), and BoHV-1 replication was enhanced by histone acetyltransferase (HAT) activator and inhibited by HAT inhibitor, suggesting HAT-dependent histone H3 acetylation plays an important role in BoHV-1 replication [14,15]. Unlike these viruses, however, hepatitis B virus (HBV) transcription and replication are repressed by histone deacetylase [16,17]. Increasing evidence indicates that viral infection can regulate histone methylation/demethylation and acetylation/deacetylation, plays a key role in regulating gene expression, and controls the process of viral infection at the whole genome level [18,19]. The silkworm (*Bombyx mori*) is a model lepidopteran species. Histone modification in silkworm embryonic cells can be regulated by the steroid hormone ecdysone 20-hydroxyecdysone [20], and H3K27ac at enhancers was required for transcriptional activation of ecdysone-responsive genes [21]. The peak of H3K27ac occurs near transcription start sites (TSS) of methyl-modified genes in silkworms. Previous reports indicate that histone modifications changed in silkworms after exposure to stress [22]. Ultraviolet irradiation increased H3K27me3, and the genome-wide distribution and accumulation of H3K4me3 marks in silkworm cells changed with *B. mori* nucleopolyhedrovirus (BmNPV) infection [23,24]. Changes in histone modifications are also accompanied by alterations in gene expression. The genes with high H3K4me3 enrichment expressed at high levels in BmNPV-infected cells and vice versa [24].

Changes in mRNA [25], lncRNA [26], miRNA [27], circRNA [28], and protein expression patterns [29] in silkworms infected with *B. mori* cytoplasmic polyhedrosis virus (BmCPV) have been identified at the whole genome level using multi-omics techniques. In eukaryotes, the initial expression pattern of genes at the whole genome level was determined by chromatin accessibility, which is regulated by histone modifications [30,31]. However, it remains unclear how changes in histone modifications caused by BmCPV infection affect gene expression. We use CUT&Tag-seq and RNA-seq to detect changes in H3K9me3/H3K9ac and gene expression and report changes in gene expression profiles to be associated with alterations in H3K9me3/H3K9ac modification at promoters and gene bodies. Changes in gene expression levels caused by histone modifications are closely related to BmCPV infection. These findings deepen our understanding of how BmCPV infection regulates gene expression through epigenetic modifications at the genome-wide level.

Materials and methods

Silkworm strains, cell lines, and virus

The silkworms (Dazao strain) used were provided by Jiangsu Province Silkworm Germplasm Resources Protection Bank (Suzhou, China). The silkworms were reared with mulberry leaves at 26°C with 70%–85% relative humidity. BmN cells derived from silkworm ovary were cultured in TC-100 medium (AppliChem, Darmstadt, Germany) supplemented with 10% foetal bovine serum (Gibco-BRL, Gaithersburg, Maryland, USA). Preparation of BmCPV stock solution (a lysate of 10^8 polyhedra/mL) was carried out following our previous study [32].

Samples preparation

The silkworms on the first day of the fifth instar were fed with the mulberry leaves coated with the BmCPV polyhedra suspension (1×10^7 /mL, 1 mL) for 10 h, followed by feed with fresh mulberry leaves. After 48 and 96 h, the midguts (200 mg) dissected from eight silkworms were collected and named Group CPV48 and Group CPV96, respectively. The midguts (200 mg) of corresponding healthy silkworms without challenge were used as controls (Group GUT48 and GUT96). Two copies were prepared for each sample. The samples were rapidly frozen in liquid nitrogen and stored at -80°C .

CUT&Tag-seq

The CUT&Tag assay was conducted according to previous reports [33,34]. Briefly, the midguts (200 mg) were homogenized with 1 mL XHB buffer (Novoseq, Beijing, China), followed by centrifugation for 5 min at $500 \times g$ at 4°C to obtain cell suspension (1×10^6). Concanavalin A coated magnetic beads (Novoseq, Beijing, China) were added to bind to cells. The bead-bound cells were resuspended in Dig-wash Buffer (20 mM HEPES pH 7.5; 150 mM NaCl; 0.5 mM Spermidine; $1 \times$ Protease inhibitor cocktail; 0.05% Digitonin) with 2 mM EDTA and anti-H3K9me3 or anti-H3K9ac antibody (Cell Signaling Technology, Boston, US), followed by incubation overnight at 4°C . After removing the unbound antibody, the cells were resuspended in Dig-wash Buffer containing Guinea-pig-anti-rabbit antibody (Thermo Fisher, Massachusetts, US) and incubated for 30 min, then with pA-Tn5 transposase (Novoseq, Beijing, China) for 1 h. To remove free pA-Tn5 transposase, the cells were placed on a magnetic rack and washed with 1 mL Dig-wash buffer

three times for 5 min each time. Finally, the DNA bound to the target protein was purified by the phenol-chloroform method [34].

To amplify libraries, the DNA obtained by CUT&Tag assay was amplified by PCR using a universal i5 and a uniquely barcoded i7 primer [35]. The PCR products were purified with AMPure beads (Beckman Coulter, California, USA) and were tested by Agilent Bioanalyzer 2100 (Novoseq, Beijing, China) to evaluate the library quality. The libraries were sequenced on the Illumina Novaseq platform (Novoseq, Beijing, China) by Beijing Nuohe Zhiyuan Technology Co., Ltd. All sequencing were deposited in the NCBI database (Supplemental Table S1).

CUT&Tag-seq data processing and bioinformatics analysis

Raw reads were assessed by FastQC (version 0.11.5) software, followed by processing with Fastp software (version 0.20.0) using a parameter with `length_required = 50`; `n_base_limit = 6` to obtain the clean reads. The obtained clean reads were further assessed by Q20, Q30, and GC content.

The clean reads were aligned to reference (*B. mori*) genome (<https://silkgdb.bioinfotoolkits.net>) using Burrows-Wheeler Aligner (BWA, version 0.7.12) software with specific parameters (`-T 25, -k 18`). The reads with mapping quality ≥ 13 were used to further analyse.

To identify regions with signal enrichment or “peaks” for each library, MACS2 (version 2.1.0) software [36] was applied for peak calling using a parameter with `macs2 -q 0.05 -f AUTO -call-summits -nomodel -shift -100 -extsize 200 -keep-dup all`. By default, the peaks with $q\text{-value} \leq 0.05$ were used for all data sets.

The findMotifsGenome.pl program in HOMER (v4.11) software [37] was used to identify conservative motifs of peaks (3000 bp upstream of transcription start site (TSS), gene bodies, transcription end sites (TES)) with `“-len 8,10,12,14 -gc -size given -homer2 -dumpFasta”`. To visualize the CUT&Tag signals intensity at specific genomic regions such as TSS, gene bodies, TES, and peaks, normalized signals from individual libraries were conducted using the computeMatrix module of DeepTools software [38].

Peaks from pooled replicates were merged using deepTools [38], and the mean RPM (Reads per million mapped reads) from each group was calculated. The peaks with foldchange of RPM more than two were considered as differential peaks. Genes related to differential peaks were screened using ChIPseeker [39].

Gene Ontology (GO) enrichment analysis for differential peak-related genes was conducted by the GOrse

R package [40]. Kyoto Encyclopedia of Genes and Genomes (KEGG) pathway (<http://www.genome.jp/kegg/>) analysis was performed using KOBAS software [41]. GO terms and pathways with corrected p-values less than 0.05 were considered significant.

Analysis of RNA-seq data

Total RNAs for library preparation were extracted from midguts (200 mg) by Trizol Reagent (Sangon Biotech, Shanghai, China) and checked by Agilent 2100 bioanalyzer. Transcriptome library construction was conducted according to the previous report [36]. The library was sequenced on the Illumina Novaseq platform (Novoseq, Beijing, China) by Beijing Nuohe Zhiyuan Technology Co., Ltd. All sequencing were deposited in the NCBI database (Supplemental Table S1). RNA-seq data processing, mapping clean reads to the *B. mori* genome, differentially expressed genes (DEGs) and gene function annotation were performed according to previous reports [40,41].

Integrative analysis of CUT&Tag-seq and RNA-seq

The computeMatrix modules of DeepTools software were used to calculate the average signal intensities of CUT&Tag of each sample at 3000bp upstream of TSS, gene body, and 3000bp downstream of TES, respectively, under a resolution 50 bp bin size [38]. Scatter plots were constructed using the gene expression levels represented by Fragments Per Kilobase of exon model per Million mapped fragments (FPKM) and the CUT&Tag signals represented by the log₂RPM at the promoter regions (2000 bp upstream and downstream of TSS) to assess the correlation between gene expression and histone modification. The genes were divided into five classes according to their expression levels and defined genes with FPKM values of 0–1 as non-expressing genes, the remaining genes were classified into four classes based on the quartiles more than 18.76, 7.00–18.76, 2.94–7.00, and 1–2.94 of the overall FPKM value. The distribution of CUT&Tag signals of genes with different expression levels at 3000 bp upstream of TSS, gene body, and 3000bp downstream of TSS was used to detect the effect of histone marks on gene expression. A heatmap, which was generated by using the median values of Log₁₀ transformed FPKM of RNA seq for DEGs (up-regulated, down-regulated, and non-differentially expressed genes) and the corresponding median values of Log₁₀ transformed RPM of CUT&Tag signals, to analyse the association between dynamic H3K9me3/H3K9ac modifications and dynamic gene transcription [42]. The cumulative

fraction curve and boxplot were generated by using log₂foldchange of CUT&Tag-seq RPM values at the promoter regions for three classes of genes (up-regulated, down-regulated, and non-differentially expressed genes). The cumulative fraction curve of log₂foldchange of RNA-seq FPKM values of genes related to CUT&Tag differential peaks (up-regulated, down-regulated, and non-differential peaks) to analyse of the association between differential H3K9me3/H3K9ac signalling and DEGs according to the previous report [43]. The Kolmogorov-Smirnov Goodness of Fit Test (K-S test) was used to examine the significant differences in the log₂foldchange mentioned above. Moreover, the log₂foldchange of RNA-seq FPKM values and log₂foldchange of CUT&Tag-seq RPM values were used in the four-quadrant graph to screen the intersection between DEGs and differential peak-related genes [43].

SDS-PAGE and Western blot

The total proteins extracted from BmCPV-infected midguts (CPV48 and CPV96) and their corresponding healthy midguts (GUT48 and GUT96) were, respectively, mixed with 5 × SDS loading buffer (Beyotime, Beijing, China) and incubated in 100°C for 10 min, then subjected to SDS-PAGE with 5% stacking gel and 12% separating gel. Western blot was conducted by using rabbit anti-H3K9me3 (Abclonal, Wuhan, China), anti-H3K9ac (Abclonal, Wuhan, China) and anti-H3 (Abclonal, Wuhan, China) antibodies as the primary antibodies, and the HRP-labelled goat anti-rabbit IgG was used as the secondary antibody (Proteintech, Shanghai, China). Histone 3 was used as an internal control [44–46]. All of the experiments were repeated three times.

Chromatin immunoprecipitation (ChIP), ChIP-qPCR and qPCR

The ChIP assay was conducted using the ChIP Assay Kit (Beyotime Biotech, Shanghai, China) according to the product description. Briefly, the midguts were cut into 1–3 mm³ in size. After 1× PBS was added into the 15 mL centrifuge tubes (10 mL PBS per gram tissue), formaldehyde saturated solution was added to the final concentration of 1.5% for cross-linking. To terminate the cross-linking reaction, glycine was added at a final concentration of 0.125 M in the total solution, followed by rotation for 5 min. Subsequently, the supernatant was discarded after centrifugation at 1000 rpm for 5 min. The precipitate was washed with 5 mL of cooled PBS for five times. The obtained precipitate was

dispensed into 1.5 mL centrifuge tubes (30 mg tissue per tube) and was added with cooled PBS. Then, the grinder (Kimble Chase New Jersey USA) was used to grind the precipitate for 2–3 min. After centrifugation at $500 \times g$ for 3 min, the supernatant was discarded. The above steps were repeated 3–5 times. The precipitate was resuspended with a 1 mL cooled PBS to obtain the cell suspension. Then, the cell suspension was filtered with a cell sieve (100 μ m). The filtrate was centrifuged at $500 \times g$ for 3 min and the supernatant was discarded. The collected cells were resuspended to the concentration of 1×10^4 cells/mL with SDS lysis Buffer (Beyotime Biotech, Shanghai, China) for complete lysis. Subsequently, the ultrasonic crushing was carried out by the UP200S ultrasonic crusher (Xinzhi Biological Company, Zhejiang, China) with the condition of 40% intensity and 9.0 sec/5.0 sec for 15 min. The supernatant was collected after centrifugation at 12,000 rpm for 5 min. Then, 1.8 mL ChIP Dilution Buffer (Beyotime Biotech, Beijing, China) containing 1 mM PMSF was added into the supernatant. Wherein 20 μ L mixture was used as input for follow-up detection. The remaining mixture was added with 5 μ L anti-H3K9me3/H3K9ac antibody (Abcam, Cambridge, England) for slow rotation overnight at 4°C. In order to precipitate proteins or corresponding complexes recognized by anti-H3K9me3/H3K9ac antibody, 60 μ L Protein A+G Agarose/Salmon Sperm DNA (Beyotime Biotech, Beijing, China) was added for 1-h slow rotation at 4°C. Then, the supernatant was removed after centrifugation at 1000 g for 1 min at 4°C. The precipitate was washed with Low Salt Immune Complex Wash Buffer (Beyotime Biotech, Beijing, China), High Salt Immune Complex Wash Buffer (Beyotime Biotech, Beijing, China), LiCl Immune Complex Wash Buffer (Beyotime Biotech, Beijing, China) once and was washed with TE Buffer (Beyotime Biotech, Beijing, China) twice in sequence (1 mL washing solution were added for 5-min slow rotation at 4°C, and were removed by 1-min centrifugation with speed of $1000 \times g$ at 4°C). The washed precipitate was resuspended with 250 μ L Elution Buffer (1%SDS and 0.1 M NaHCO₃) twice. The collected supernatant (approximately 500 μ L) was incubated with 20 μ L 5 M NaCl for 4 h at 65°C. Meanwhile, the Input sample was incubated with 1 μ L 5 M NaCl for 4 h at 65°C so as to obtain Input DNA. After that, the sample was incubated with 10 μ L 0.5 M EDTA, 20 μ L 1 M Tris (pH=6.5) and 1 μ L protease K(20 mg/mL) for 1 h at 45°C. Next, the equal volume of phenol was added to the mixture for mixing by a vortex. The phenol-chloroform method was used to purify DNA. To verify the level of histone modification, qPCR was carried out

with the purified DNA and Input DNA as templates. The primers were listed in Supplemental Table S2. All experiments were repeated three times. The $2^{-\Delta\Delta Ct}$ method was used to calculate the relative histone modification level of the target genes. The calculation formulas were as follows [47]:

$$\Delta Ct_{[\text{normalized ChIP}]} = (Ct_{[\text{ChIP}]} - (Ct_{[\text{Input}]} - \log_2 (\text{Input Dilution Factor})))$$

Input Dilution Factor(IDF) = (fraction of the Input chromatin saved) – 1

$$\Delta\Delta Ct_{[ChIP/NIS]} = \Delta Ct_{[\text{normalized ChIP}]} - \Delta Ct_{[IgG]}$$

$$\text{Fold Enrichment} = 2^{(-\Delta\Delta Ct_{[ChIP/NIS]})}$$

The total RNAs were extracted from the BmCPV-infected midguts (CPV48 and CPV96) as well as corresponding healthy silkworms (GUT48 and GUT96) using TransScript® One-Step gDNA Removal (TransGen Biotech, Beijing, China), and the cDNA was synthesized with cDNA Synthesis SuperMix kit (TransGen Biotech, Beijing, China). Subsequently, the cDNA was used as a template, and the expression level of the BmCPV *vp1* gene was determined by real-time PCR with the specific primer pairs (Supplemental Table S3) using TransStart® Tip Green real-time PCR SuperMix (TransGen Biotech, Beijing, China). The housekeeping gene translation initiation factor 4A (TIF-4A) of *B. mori* was used as an internal control for normalization. The $2^{-\Delta\Delta Ct}$ method was used to calculate the relative expression level of the target gene [48]. Each experiment was repeated three times.

Statistical analysis

Data analysis was performed with SPSS software ver. 28.0 (SPSS, Inc., Chicago, USA) and GraphPad Prism 8.0 (GraphPad Software, LaJolla, USA). All experimental data are expressed as the mean \pm s.e.m. Paired t-test was used for statistical analysis (ns, $p > 0.05$; * $p < 0.05$; ** $p < 0.01$; *** $p < 0.001$).

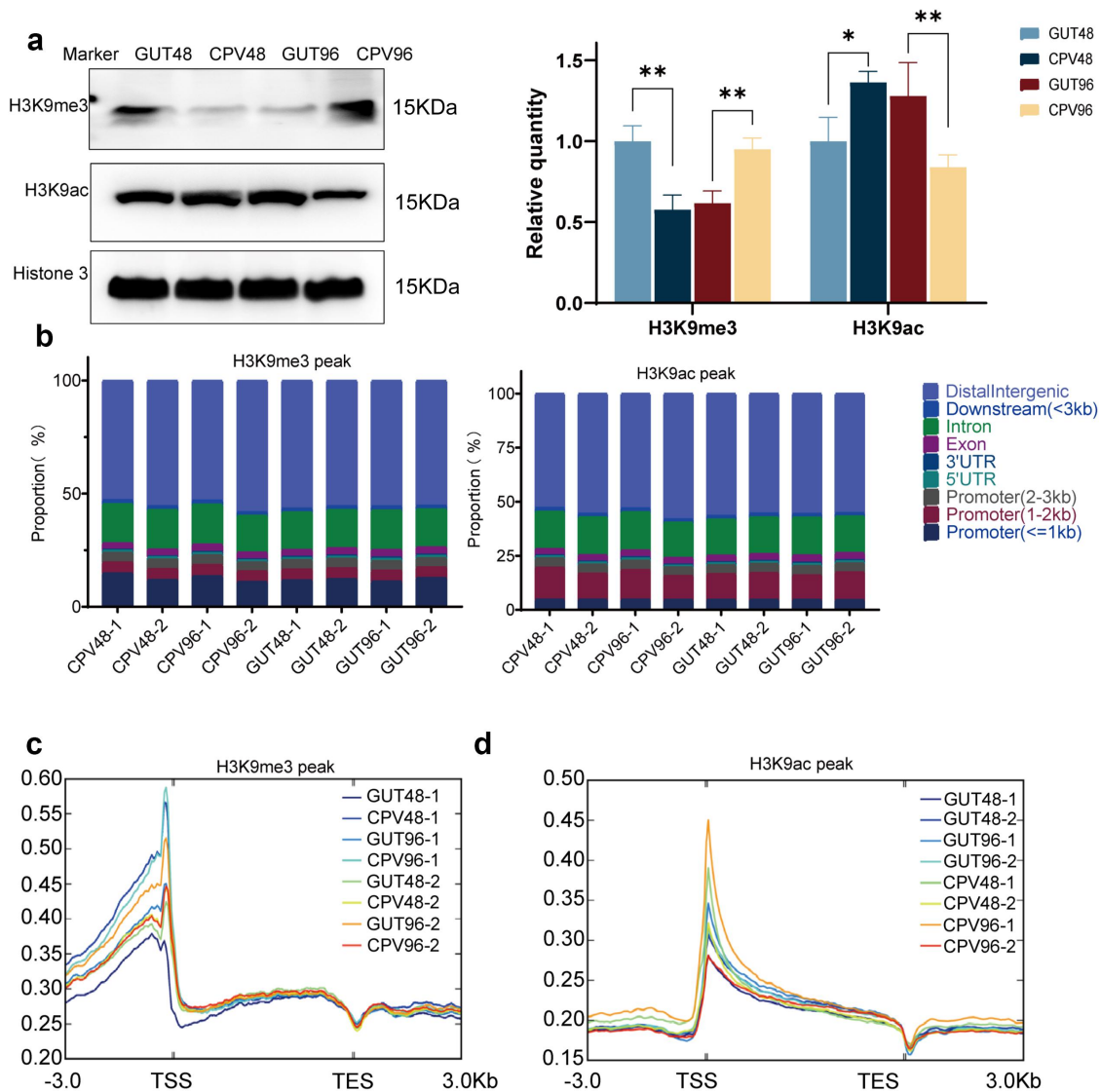


Figure 1. Effects of BmCPV infection on H3K9me3 and H3K9ac in the silkworm midgut. (a) H3K9me3 and H3K9ac were detected by Western blot in the midgut of 5th instar silkworms infected with BmCPV at 48 and 96 h post-infection and corresponding healthy silkworms. Histone H3 was used as an internal reference. The first antibody was a rabbit anti-H3K9me3 antibody (1:1000) and rabbit anti-H3K9ac antibody (1:1000), and the second antibody was the HRP-conjugated goat anti-rabbit IgG (1:5000). Left, Western blot detection of H3K9me3 and H3K9ac; right, grayscale results of signaling bands of Western blot; lane CPV48 and CPV96, the midgut of 5th instar silkworms infected with BmCPV at 48 and 96 h post-infection; lane GUT48 and GUT96, the midgut corresponding healthy silkworms without infection, the experiments were repeated three times ($*p < 0.05$; $**p < 0.01$). (b) The distribution of H3K9me3/H3K9ac peaks in different regions of the genome. The X axis was the sample name and the Y axis was the proportion of functional regions. (c,d) The distribution of H3K9me3 and H3K9ac peaks in the genome. The X axis was the position of reads in the genome and the Y axis was the density of reads. TSS, transcription start sites; TES, transcription end sites.

Results

BmCPV infection regulates H3K9me3/H3K9ac modification levels in the silkworm

BmCPV specifically infects silkworm midgut epithelial cells. To verify if histone modifications can be regulated by BmCPV infection, we examined changes in H3K9me3 and H3K9ac levels in the midgut of

BmCPV-infected silkworm by Western blot. Levels of H3K9me3 in Group CPV48 were lower than levels in Group GUT48; levels in Group CPV96 were higher than those in Group GUT96 and levels in Group CPV96 were higher than those in Group CPV48, while the changes in H3K9ac levels were just the opposite (Figure 1(a) and Supplemental Figure S1).

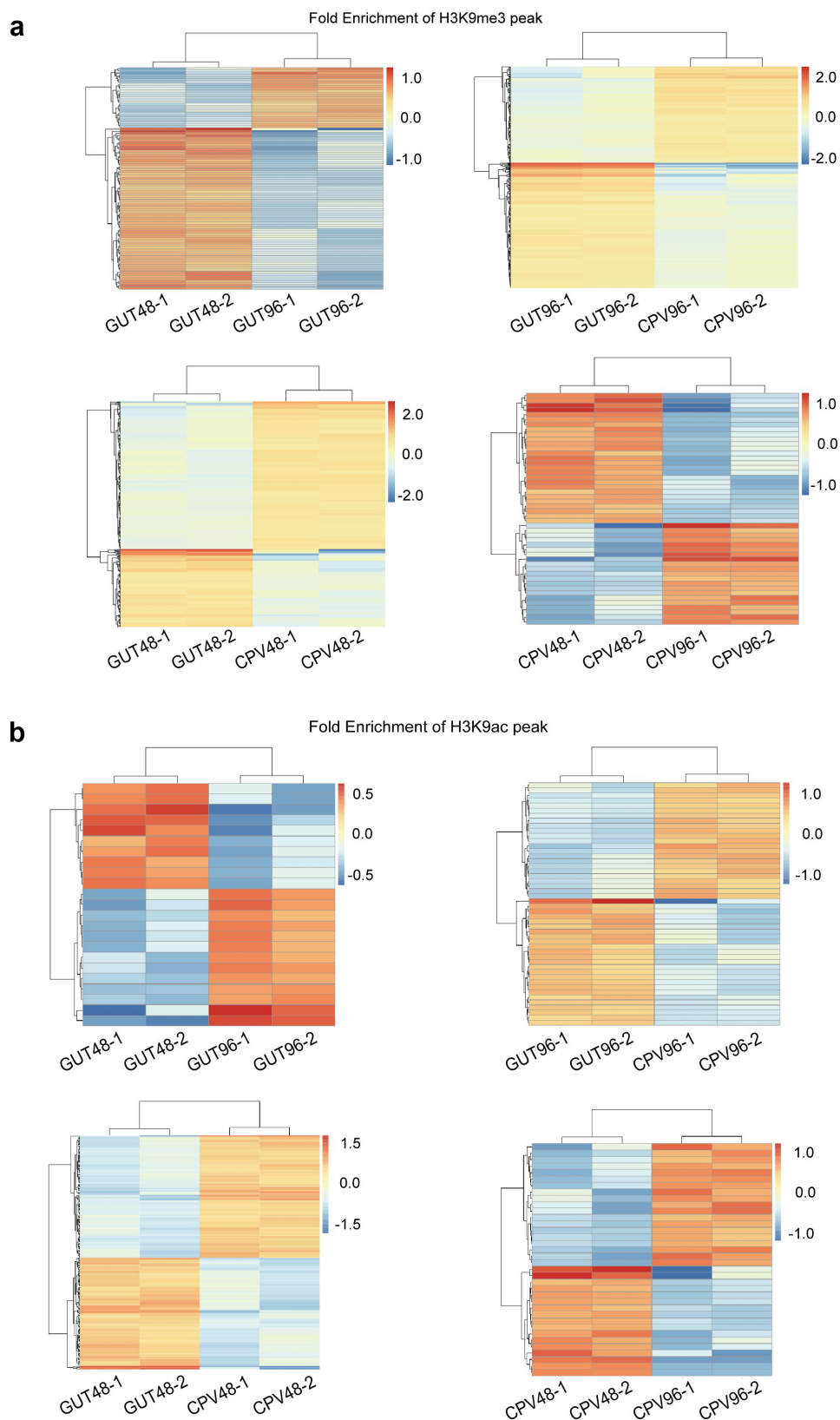


Figure 2. Identification of differential H3K9me3 and H3K9ac peaks. (a) Cluster analysis of the enrichment multiples of H3K9me3 peaks between four groups, including GUT96 vs GUT48, CPV48 vs GUT48, CPV96 vs GUT96 and CPV96 vs CPV48 group. The logo in the upper right corner indicated the enrichment multiple. The greater the upregulation multiple, the darker the red; the greater the downregulation multiple, the darker the blue. each row represents a H3K9me3-enriched peak. (b) Cluster analysis of the enrichment multiples of H3K9ac peaks between four groups, including GUT96 vs GUT48, CPV48 vs GUT48, CPV96 vs GUT96 and CPV96 vs CPV48 group. each row represents a H3K9ac-enriched peak.

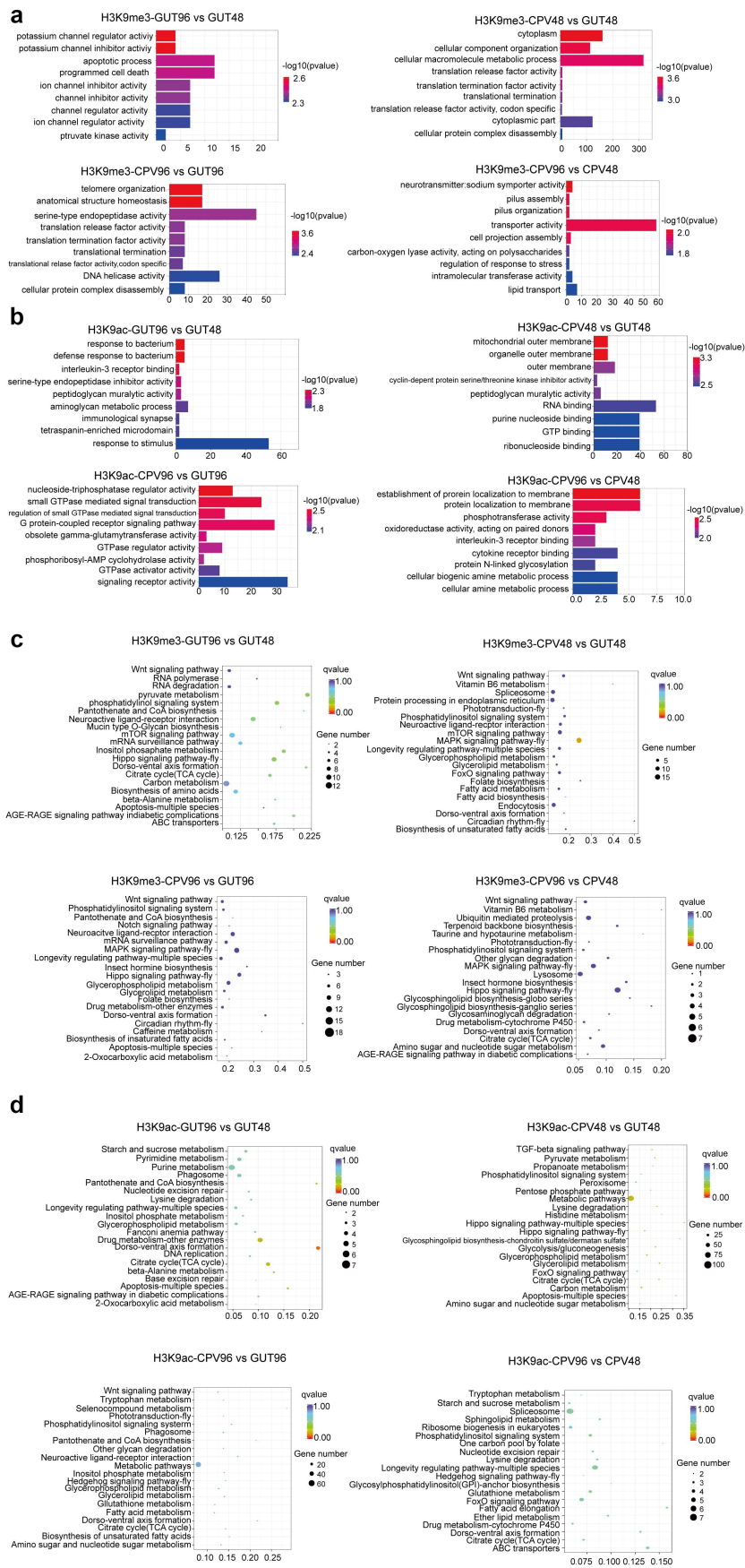


Figure 3. GO and KEGG enrichment of differential H3K9me3 peaks and H3K9ac peaks. (a,b) Top 10 go terms related to differential H3K9me3 peaks and H3K9ac peaks, respectively. The X-axis represented the number of genes enriched in the GO term, and the

BmCPV infection changes H3K9me3/H3K9ac modification profiles in silkworm midguts

H3K9me3 and H3K9ac modification profiles in Group CPV48, Group CPV96, Group GUT48 and Group GUT96 ($n = 2$) were determined using CUT&Tag. Raw and clean reads and the ratios of clean and mapped reads for each sample were presented in Supplemental Table S4. Obtained data met requirements for further analysis.

To characterize histone modification profiles, global enrichment of H3K9me3/H3K9ac modification was determined using the percentage of the genome covered by peaks in both replicates (Supplemental Figure 2 and Supplemental Figure 3). Coverage of identified H3K9me3 (H3K9ac values in parentheses) peaks was about 43–46% (50–60%) for the distal intergenic region, 30–40% (20–25%) for promoters, 10–12% (16–18%) for introns, and 6–8% (2–4%) for exons (Figure 1(b)).

Average signal intensities of H3K9me3/H3K9ac peaks occurred at gene bodies (transcripts scaled to 3000 bp upstream and 3000 bp downstream regions) peaked at TSS and were lowest at TES. However, signal intensity differed in the midguts of BmCPV-infected and non-infected silkworms (Figure 1(c,d)). To understand the regulatory effect of BmCPV infection on H3K9me3/H3K9ac, cluster analysis of the enrichment multiples of H3K9me3/H3K9ac peaks between four groups, including GUT96 vs GUT48, CPV48 vs GUT48, CPV96 vs GUT96, and CPV96 vs CPV48, was performed. Results show that H3K9me3/H3K9ac changed with silkworm development and BmCPV infection (Figure 2(a,b)). The H3K9me3 enrichment pattern in the GUT96 vs GUT48 group is opposite that of the H3K9ac enrichment pattern in the GUT96 vs GUT48 group (Figure 2(a,b)). Similarly, the number of H3K9me3-upregulated peaks is more than that of H3K9me3-downregulated peaks, while the number of H3K9ac-upregulated peaks is less than that of H3K9ac-downregulated peaks (Supplemental Figure 4). BmCPV infection increased differential H3K9me3 and H3K9ac peaks (Figure 2(a,b)). Although the H3K9me3 enrichment pattern in CPV48 vs GUT48 groups is contrary to that in CPV96 vs GUT96 group, the numbers of H3K9me3-

upregulated peaks in CPV48 vs GUT48 group and CPV96 vs GUT96 group both exceed that of H3K9me3-downregulated peaks (Supplemental Figure 4(a)). The H3K9ac enrichment pattern in the CPV48 vs GUT48 group is similar to that in CPV96 vs GUT96 group (Figure 2(b)). Numbers of H3K9ac-upregulated peaks in both groups exceed downregulated peaks (Supplemental Figure 4(b)). In the CPV96 vs CPV48 group, the H3K9me3 enrichment pattern is opposite that of the H3K9ac enrichment pattern in the GUT96 vs GUT48 group (Figure 2(a,b)), although numbers of H3K9me3- and H3K9ac-upregulated peaks both exceed that of H3K9me3- and H3K9ac-downregulated peaks (Supplemental Figure 4). Changes in levels (up or down) of regulation of differential peaks in H3K9ac differed from those in H3K9me3, suggesting that H3K9me3/H3K9ac modification profiles in the silkworm midgut were altered by BmCPV infection.

Differential H3K9me3/H3K9ac-peak-related genes are associated with BmCPV infection

To understand differential H3K9me3/H3K9ac-peak-related genes caused by BmCPV infection, gene ontology (GO) enrichment analysis was performed. GO terms annotated to differential H3K9me3-peaks in the GUT96 vs GUT48 comparison were mainly enriched into potassium channel regulator activity, potassium channel inhibitor activity, and apoptotic process. The main enriched GO terms in the CPV48 vs GUT48 comparison were cytoplasm, cellular component organization, and cellular macromolecule metabolic process. Those for the CPV96 vs GUT96 comparison were telomere organization, anatomical structure homeostasis, and serine-type endopeptidase activity. For the CPV96 vs CPV48 comparison these were neurotransmitter transporter activity, neurotransmitter: sodium symporter activity, pilus assembly/pilus organization, and transporter activity (Figure 3(a)). For H3K9ac, the main GO terms annotated to differential H3K9ac-peaks in the GUT96 vs GUT48 comparison were response to bacterium, defence response to bacterium, and interleukin-3 receptor binding; those for the CPV48 vs GUT48 comparison were mitochondrial

Y-axis represented the GO term. (c,d) KEGG enrichment of differential H3K9me3 peaks and H3K9ac peaks, respectively. The X-axis represented rich factors and the Y-axis represented KEGG enrichment pathways. The smaller the p-value, the higher the significance of enrichment. The number of genes is represented by the size of a dot, with larger dots indicating more genes. Rich factor, the ratio of the number of genes with differential H3K9me3/H3K9ac peaks in this pathway term to the number of all genes in this pathway term.

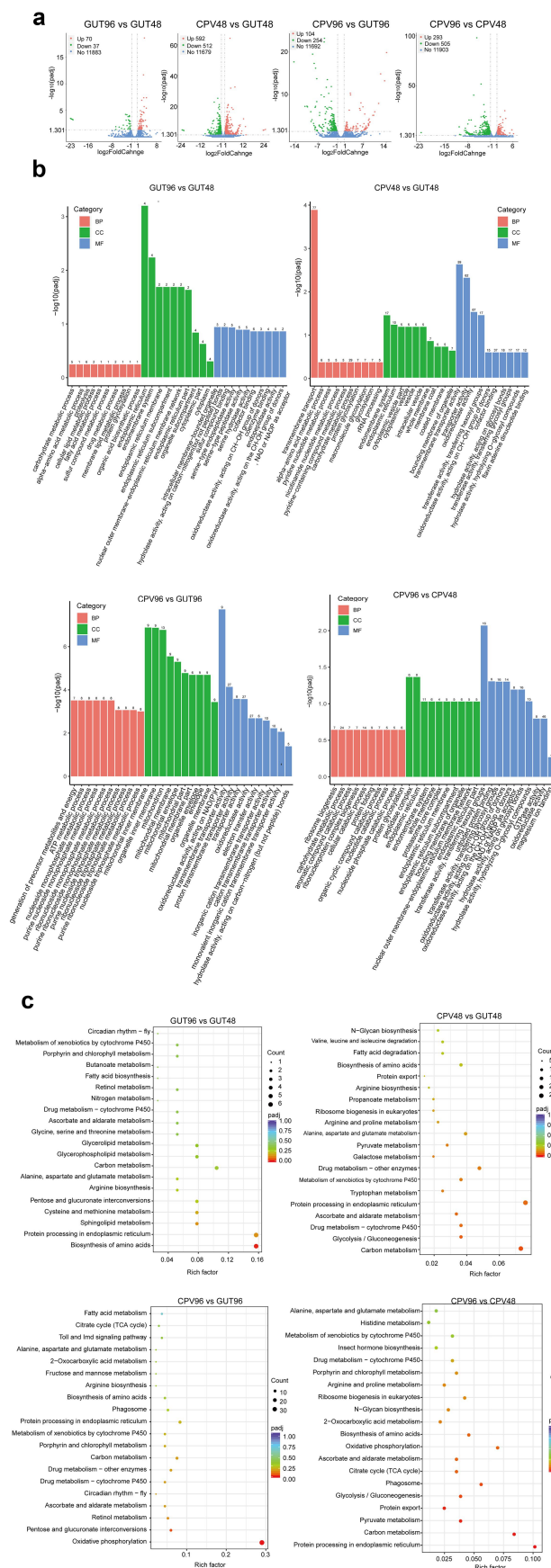


Figure 4. Overview of RNA-seq data. (a) The volcano plots of DEGs in GUT96 vs GUT48, CPV48 vs GUT48, CPV96 vs GUT96, and CPV96 vs CPV48 groups, respectively. The X-axis represented the expression level of DEG \log_2 foldchange, and the Y-axis represented

outer membrane, organelle outer membrane, and outer membrane. The main enriched GO terms in the CPV96 vs GUT96 comparison were nucleoside-triphosphatase regulator activity, small GTPase mediated signal transduction, and regulation of small GTPase mediated signal transduction. Enriched GO terms for the CPV96 vs CPV48 comparison were mainly establishment of protein localization to membrane, and protein localization to membrane and phosphotransferase activity (Figure 3(b)).

KEGG enrichment analysis of differential H3K9me3-peak- and H3K9ac-peak- related genes revealed that the enriched pathways for differential H3K9me3 peaks were mainly involved in pyruvate metabolism, phosphatidylinositol signalling system, and the Hippo signalling pathway in the GUT96 vs GUT48 comparison; the MAPK and Wnt signalling pathways, and circadian rhythm in the CPV48 vs GUT48 comparison; dorso-ventral axis formation, and MAPK and Hippo signalling pathways in the CPV96 vs GUT96 comparison; and the Hippo signalling pathway, insect hormone biosynthesis, ubiquitin-mediated proteolysis, and MAPK signalling pathway in the CPV96 vs CPV48 comparison (Figure 3(c) and Supplemental Table S5).

For differential H3K9ac peak-related genes, the main enriched KEGG pathways were dorso-ventral axis formation, citrate cycle (TCA cycle), and pantothenate and CoA biosynthesis in the GUT96 vs GUT48 comparison; Hippo signalling pathway – multiple species, apoptosis-multiple species, and the citrate cycle (TCA cycle) in the CPV48 vs GUT48 comparison; neuroactive ligand–receptor interaction, dorso-ventral axis formation, and pantothenate and CoA biosynthesis in the CPV96 vs GUT96 comparison; and ABC transporters, longevity regulating pathway-multiple species, dorso-ventral axis formation, and fatty acid elongation in the CPV96 vs CPV48 comparison (Figure 3(d) and Supplemental Table S6). Significant changes have occurred in GO and KEGG enrichment of differential H3K9me3/H3K9ac-peak-related genes following BmCPV infection, suggesting that these genes are associated with BmCPV infection.

Association of DEGs with BmCPV infection

To understand the response of gene expression profile to BmCPV infection at the whole genome level, RNA-seq was performed on parallel samples from CUT&Tag-seq. Basic RNA-Seq data and box plots of gene expression for each sample are presented in Supplemental Table S7 and Supplemental Figure 5. There were 107 DEGs ($|\log_2\text{foldchange}| > 1$) in the GUT96 vs GUT48 comparison, including 70 DEGs that were up-regulated and 37 DEGs that were down-regulated (Figure 4(a)). After BmCPV infection, the number of DEGs increased. Of the 1104 DEGs in the CPV48 vs GUT48 comparison, 592 were up-regulated and 512 were down-regulated. Of the 359 DEGs in the CPV96 vs GUT96 comparison, 104 were up-regulated and 254 were down-regulated. Of the 798 DEGs in the CPV96 vs CPV48 comparison, 293 were up-regulated and 505 were down-regulated (Figure 4(a)).

To better understand the response of silkworms to BmCPV infection, GO and KEGG enrichment analyses were performed on DEGs. GO terms were mainly enriched in endoplasmic reticulum, and endomembrane system and hydrolase activity, acting on carbon – nitrogen (but not peptide) bonds in the GUT96 vs GUT48 comparison (Figure 4(b)). Transmembrane transport, transmembrane transporter activity, and transporter activity were mainly enriched in the CPV48 vs GUT48 comparison (Figure 4(b)). Oxidoreductase activity, acting on NAD (P)H, mitochondrial inner membrane, and organelle inner membrane was mainly enriched in the CPV96 vs GUT96 comparison (Figure 4(b)). Transferase activity, transferring hexosyl groups, unfolded protein binding, and transferring glycosyl groups, were mainly enriched in the CPV96 vs CPV48 comparison (Figure 4(b)).

For the GUT96 vs GUT48 comparison, KEGG enrichment analysis of DEGs revealed the main enriched pathways to be biosynthesis of amino acids, protein processing in endoplasmic reticulum, and sphingolipid metabolism (Figure 4(c) and Supplemental Table S8). For the CPV48 vs GUT48 comparison, DEGs were mainly enriched in carbon

the adjusted p-value ($-\log_{10}\text{padj}$), and the dashed line represented the threshold line for screening differential genes. The red dots represented up-regulated genes, the green dots represented down-regulated genes and the blue dots represented non-differentially expressed genes. (b) GO enrichment of DEGs. The top 30 GO terms were enriched in GUT96 vs GUT48, CPV48 vs GUT48, CPV96 vs GUT96 and CPV96 vs CPV48 groups, respectively. The X-axis represented GO terms and the Y-axis represented the adjusted p-value ($-\log_{10}\text{padj}$). The numeral over the bar represented the number of DEGs annotated to this GO term. The red, green and blue bars represented GO terms belonging to biological process (BP), cellular component (CC) and molecular function (MF), respectively. (c) KEGG enrichment of DEGs. The X-axis represented rich factors and the Y-axis represented KEGG enrichment pathways. The smaller the p-value, the higher the significance of enrichment. The number of genes is represented by the size of a dot, with larger dots indicating more genes.

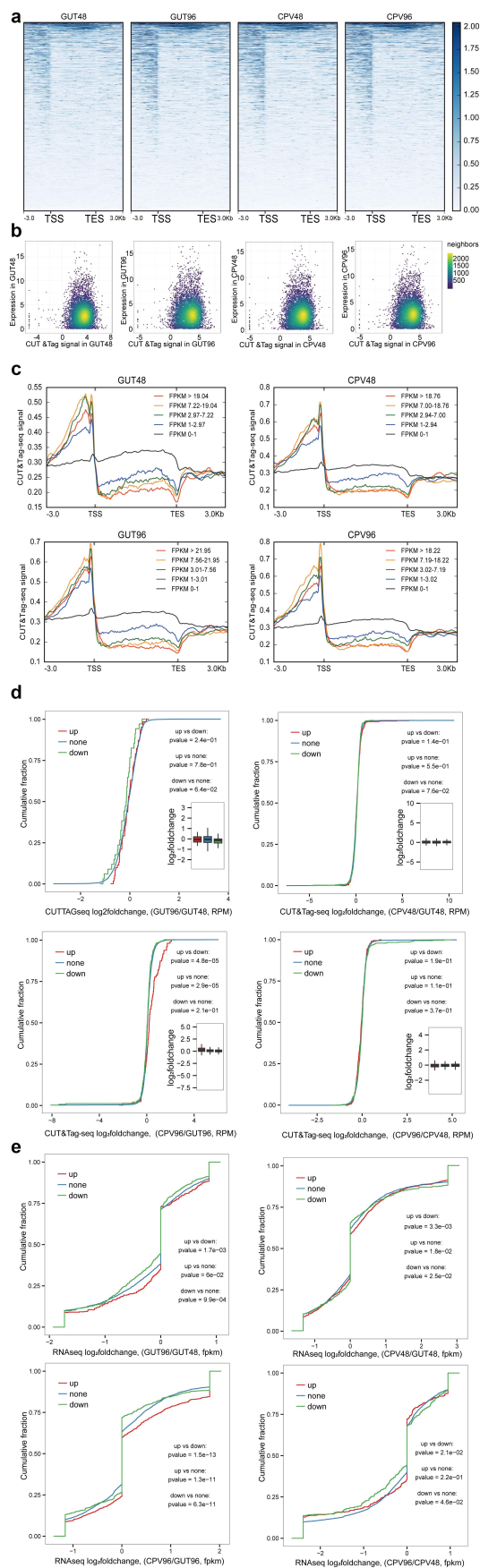


Figure 5. Association analysis of differential H3K9me3-peak and DEGs. (a) Heatmap of all CUT&Tag-seq signals for H3K9me3 from 3000 bp upstream of the TSS to 3000 bp downstream from the TES of genes. TSS, transcription start sites; TES, transcription end

metabolism, protein processing in endoplasmic reticulum, and glycolysis/gluconeogenesis (Figure 4(c) and Supplemental Table S8). For the CPV96 vs GUT96 comparison, the most significantly enriched pathways were oxidative phosphorylation, then pentose and glucuronate interconversions, and retinol metabolism (Figure 4(c) and Supplemental Table S8). The main enriched KEGG pathways in the CPV96 vs CPV48 comparison were protein processing in endoplasmic reticulum, carbon metabolism, and pyruvate metabolism (Figure 4(c) and Supplemental Table S8). Overall, following BmCPV infection, significant changes occurred in the GO terms and KEGG enrichment pathways of DEGs in the midgut of silkworms, indicating that DEGs are involved in the virus–host interaction.

Changes in gene expression level caused by alteration of H3K9me3 modification levels are associated with BmCPV infection

To understand the regular roles of H3K9me3 modification on gene expression, we performed an integration analysis between differential H3K9me3 peaks and DEGs. We first characterized the distribution of CUT&Tag-seq peak signals for all genes. Read densities of H3K9me3 modification intensity surrounded TSS and gene bodies (transcripts scaled to 3000 bp upstream and 3000 bp downstream) (Figure 5(a)). Scatter plots of correlations between all CUT&Tag-seq signals (\log_2 RPM) for H3K9me3 in promoter regions (2000 bp upstream and downstream of TSS) and all gene expression levels revealed a relationship between gene expression levels and their H3K9me3 modification level (Figure 5(b)). The distribution of CUT&Tag-seq signals of genes with different expression levels revealed gene expression level to correlate weakly and positively with the intensity of CUT&Tag-seq signals in the upstream 3000 bp region of TSS, negatively with the

intensity of CUT&Tag-seq signals in the TSS to TES region and to not significantly correlate with the intensity of CUT&Tag-seq signals in the downstream 3000 bp region of TES (Figure 5(c)). A heatmap was generated using median values of \log_{10} transformed FPKM of RNA seq for DEGs and the corresponding median values of \log_{10} transformed RPM of CUT&Tag-seq signals in promoters. The increase in H3K9me3 modification level in promoters, to some extent, increased gene expression level (Supplemental Figure 6).

To determine if there was an accompanying change in H3K9me3 modification with genes with significant changes in transcription levels, the cumulative fraction of \log_2 foldchange of CUT&Tag-seq RPM values at promoter regions for differentially up-regulated, down-regulated, and non-differentially expressed genes were calculated. An increase in H3K9me3 modification in the promoter region promoted corresponding gene expression levels in the CPV96 vs GUT96 and GUT96 vs GUT48 comparisons (Figure 5(d)). Similar results were obtained by estimating the cumulative fraction of \log_2 foldchange of gene expression level with up-regulated, down-regulated, and non-differentially H3K9me3-peaks (Figure 5(e)). These results suggest that changes in gene expression profiles were associated with alteration of H3K9me3 modification in the promoter region.

The \log_2 foldchange of both CUT&Tag-seq peak and RNA-seq FPKM was used to assess correlations between changes in H3K9me3 modification and gene expression and to identify intersection genes between them [43]. For the GUT96 vs GUT48, CPV48 vs GUT48, CPV96 vs GUT96, and CPV96 vs CPV48 comparisons there were 5, 118, 54 and 40 intersection genes (Figure 6(a)). To understand intersection gene functions, KEGG annotation and enrichment analyses were performed. Intersection genes were enriched in circadian rhythm and neuroactive ligand-receptor

sites. (b) Scatter plots of the correlations between all CUT&Tag signals for H3K9me3 and all gene expression levels in promoter regions. The X-axis represented CUT&Tag-seq signal levels for H3K9me3 (\log_2 RPM of the promoter region), and the Y-axis represented gene expression levels (FPKM). The yellower the dot was, the stronger the relevance between gene expression level and CUT&Tag-seq in promoter was. Due to the presence of two biological replicates in each group, the average value of all replicates within that group was taken. (c) CUT&Tag signal distribution of genes from RNA-seq. Genes from RNA-seq were classified into one of five bins based on their FPKM values. The X-axis represented gene regions (from 3000 bp upstream of the TSS to 3000 bp downstream from the TESs) and the Y-axis represented average CUT&Tag signals for H3K9me3 (RPM). TSS, transcription start sites; TES, transcription end sites. (d) Cumulative distribution function (CDF) plots and boxplots of three groups of genes. The genes were divided into up-, non- and down-regulated genes based on gene expression levels \log_2 foldchange. In CDF plots, the X-axis represented H3K9me3 CUT&Tag-seq RPM values \log_2 foldchange of up-, non- and down-regulated genes while the Y-axis represented cumulative fraction values. In boxplots, the X-axis represented three groups of genes, including up-, non- and down-regulated genes and the Y-axis represented H3K9me3 CUT&Tag-seq RPM values \log_2 foldchange. p-values were obtained by KS tests on CUT&Tag-seq RPM of three types of genes pairwise. (e) CDF plots of genes related to differential H3K9me3 peaks. The X-axis represented RNA-seq FPKM \log_2 foldchange and the Y-axis represented cumulative fraction values. p-values were obtained by KS tests on RNA-seq FPKM of three types of genes pairwise.

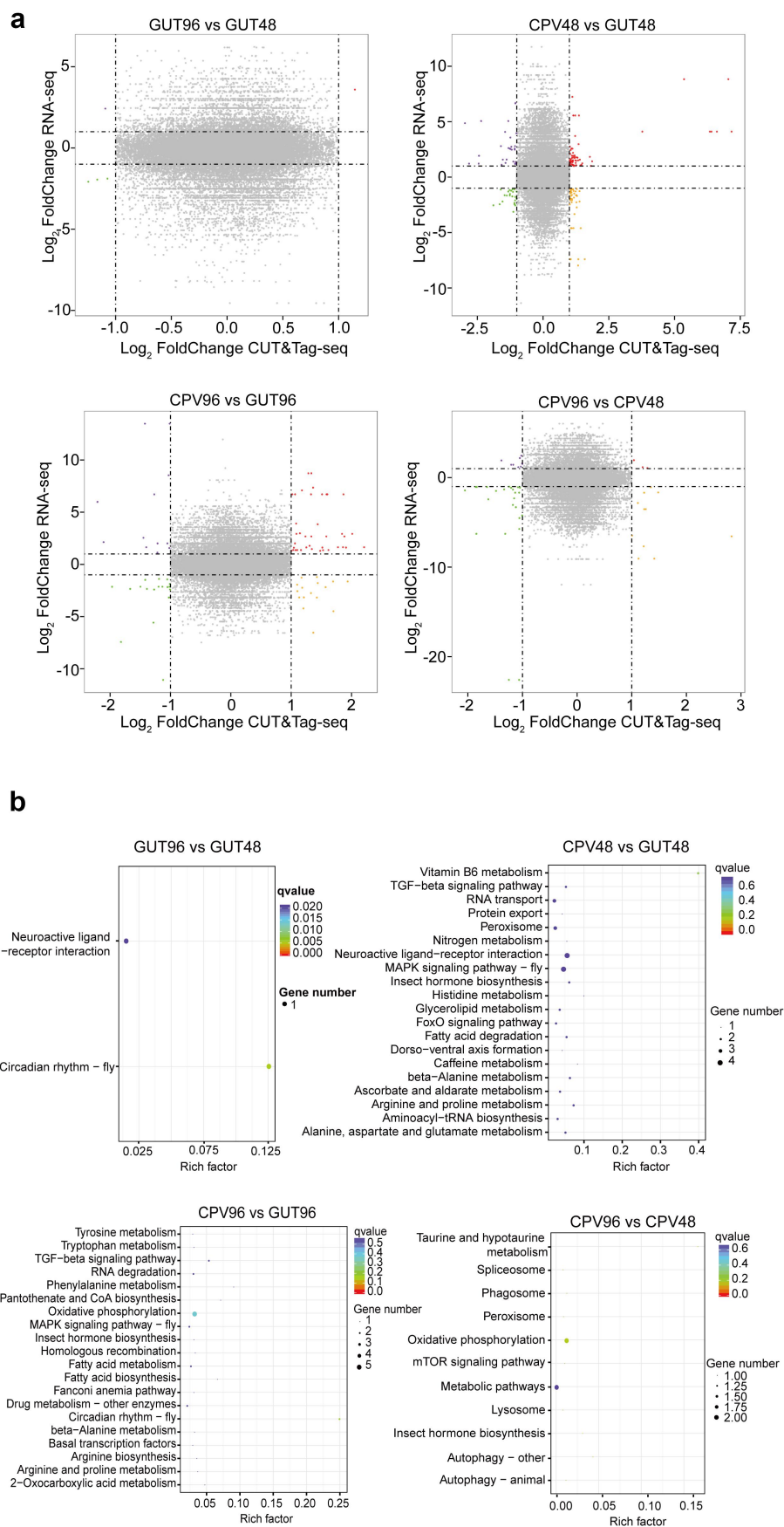


Figure 6. Identification of H3K9me3-related intersection genes. (a) Quadrantal distribution plots of H3K9me3-related and DEGs. The X-axis represented the RNA-seq FPKM log2foldchange and the Y-axis represented CUT&Tag-seq of all H3K9me3 peaks log₂

interaction in the GUT96 vs GUT48 comparison; vitamin B6 metabolism, insect hormone biosynthesis, MAPK signalling pathway, and neuroactive ligand-receptor interaction in the CPV48 vs GUT48 comparison; circadian rhythm-fly, oxidative phosphorylation, TGF-beta signalling pathway, insect hormone biosynthesis, and MAPK signalling pathway in the CPV96 vs GUT96 comparison; and taurine and hypotaurine metabolism, oxidative phosphorylation, autophagy-animal, and insect hormone biosynthesis in the CPV96 vs CPV48 comparison (Figure 6(b) and Supplemental Table S9). These results indicated that changes in intersection gene expression levels caused by H3K9me3 modification are associated with BmCPV infection.

Changes in gene expression level caused by alteration of H3K9ac modification levels are associated with BmCPV infection

To characterize correlations between H3K9ac modification and gene expression in silkworms, the distribution of H3K9ac peak signals for all genes at promoters (TSS, 3000 bp upstream and downstream of gene body regions) was examined. H3K9ac signals peaked at TSS (Figure 7(a)). Scatter plots of correlations between all CUT&Tag-seq signals (\log_2 RPM) for H3K9ac at promoters (2000 bp upstream and downstream of TSS) and all gene expression levels revealed a positive correlation between gene expression levels and their H3K9ac signals (Figure 7(b)).

The distribution of CUT&Tag-seq signals of genes with different expression levels revealed gene expression levels to correlate positively with the intensity of CUT&Tag-seq H3K9ac signals at TSS (Figure 7(c)). A heatmap generated using median values of both \log_{10} FPKM of RNA seq for DEGs and \log_{10} RPM of CUT&Tag-seq signals revealed the H3K9ac signals to correlate positively with corresponding gene expression levels (Supplemental Figure 7). Furthermore, the cumulative distribution of the \log_2 foldchange of CUT&Tag-seq RPM values of promoter regions for differentially up-, down-, and non-differentially expressed genes was used to examine if genes with significant changes in transcription levels were accompanied by changes in H3K9ac modification. H3K9ac signals promoted corresponding gene expression levels only in the GUT96 vs

GUT48 comparison (Figure 7(d)). The cumulative distribution of \log_2 foldchange of gene expression level with up-, down-, and non-differentially regulated H3K9ac peaks was used to assess the effect of changes in H3K9ac signals on corresponding gene expression. Expression levels of genes with RNA-seq (\log_2 foldchange) < 0 were promoted by H3K9ac modification in the GUT96 vs GUT48 comparison; expression levels of genes with RNA-seq (\log_2 foldchange) > 1 were inhibited by H3K9ac modification level in the CPV48 vs GUT48 comparison; expression levels of genes with RNA-seq (\log_2 foldchange) > 0 was promoted by H3K9ac modification level in the CPV96 vs GUT96 comparison; and gene expression levels were inhibited by H3K9ac modification level in the CPV96 vs CPV48 comparison (Figure 7(e)). These results suggest that not all gene expression differences are determined by H3K9ac modification levels.

The \log_2 foldchange of both CUT&Tag-seq peaks and RNA-seq FPKM were used to assess correlations between changes in both H3K9ac modification and gene expression and to identify intersection genes between them. For the GUT96 vs GUT48, CPV48 vs GUT48, CPV96 vs GUT96, and CPV96 vs CPV48 comparisons there were 2, 117, 25, and 18 intersection genes (Figure 8(a)). KEGG analysis revealed the function of intersection genes to be enriched in the FoxO signalling pathway in the GUT96 vs GUT48 comparison; glycolysis/gluconeogenesis, pyruvate metabolism, TGF-beta signalling pathway, insect hormone biosynthesis, and mitophagy-animal in the CPV48 vs GUT48 comparison; glycine, serine and threonine metabolism, cysteine and methionine metabolism, and biosynthesis of amino acids in the CPV96 vs GUT96 comparison; and phosphonate and phosphinate metabolism, circadian rhythm – fly, and protein export in the CPV96 vs CPV48 comparison (Figure 8(b) and Supplemental Table S9). These results indicate that changes in intersection gene expression levels caused by H3K9ac modification are associated with BmCPV infection.

Validation of CUT&Tag-seq data and RNA-seq data

To verify the CUT&Tag-seq data, we randomly selected eight genes with differential H3K9me3 peaks and differential H3K9ac peaks (Supplemental Table S10). Purified DNAs obtained by ChIP assay were used as

foldchange). The dashed lines represented that the absolute value of RNA-seq FPKM(\log_2 foldchange) was 1 or the absolute value of CUT&Tag-seq of all H3K9me3 peaks \log_2 foldchange was 1. (b) KEGG enrichment of intersection genes. The Y-axis represented the KEGG pathway, and the X-axis represented the rich factor. Qvalue, corrected p -value.

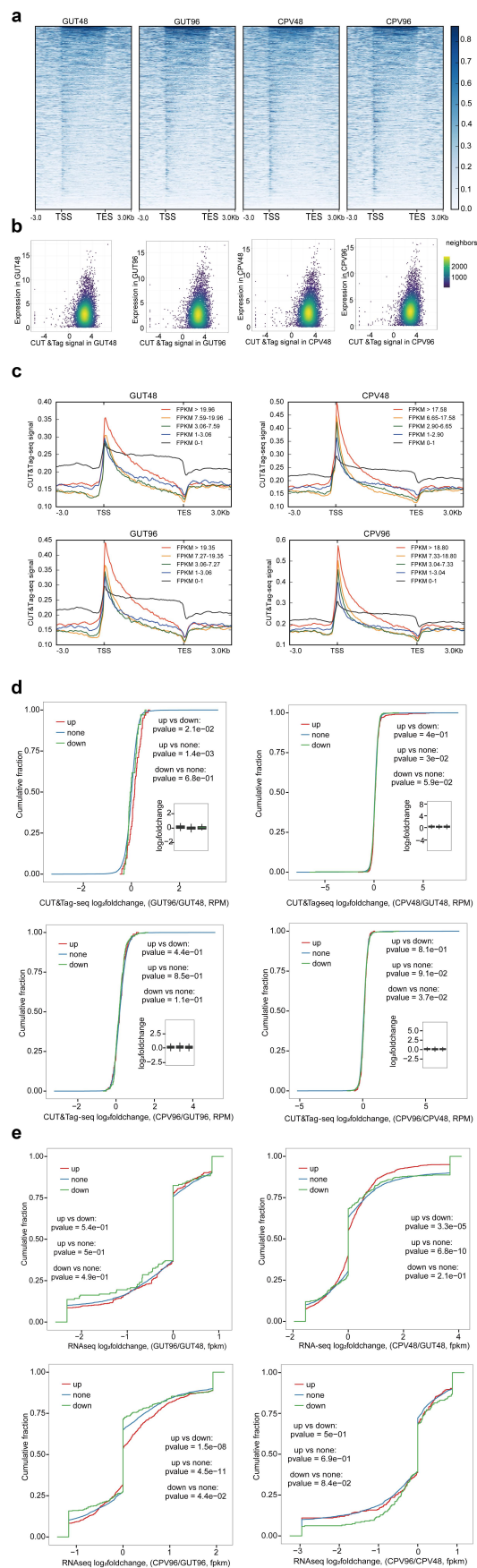


Figure 7. Association analysis of differential H3K9ac-peak and DEGs. (a) Heatmap of all CUT&Tag-seq signals for H3K9ac from 3000 bp upstream of the TSS to 3000 bp downstream from the TES of genes. TSS, transcription start sites; TES, transcription end sites. (b)

qPCR templates, with input DNA as a positive control. Changes in H3K9me3/H3K9ac levels in gene regions by ChIP-qPCR were in accordance with CUT&Tag-seq data, indicating high credibility of CUT&Tag-seq data (Figure 9(a,b) and Supplemental Table S10).

To verify reliability of RNA-seq data, we randomly selected six up- and six down-regulated DEGs in each treatment (Supplemental Table S3). The qPCR results trended in the same way as RNA-seq data, indicating the high credibility of RNA-seq data (Figure 9(c)).

Discussion

To establish infection, a virus can hijack expression of host genes by regulating histone modifications. Papilloma virus can induce rabbit epithelial cells to express arginase that causes histone arginine modification [49]. Simian vacuolating virus 40 can change levels of H3 and H4 acetylation [50]. Human T-lymphotropic virus 1 infection can cause H4 acetylation in suppression factors related to cyclin-dependent kinases, and change H3K27me3 levels in genes associated with transcription regulations, immunity responses, and cellular metabolism [51,52]. Hepatitis C virus infection mainly changes H3K9ac enrichment in cis-regulatory element regions, H3K4me3 enrichment in gene body regions, and H3K9me3 enrichment in TSS [53]. Merkel cell polyomavirus infection can down-regulate H3K27me3 [54]. High-risk human papillomavirus infection can induce down-regulation of H3K27me3 and H3K9me2, and up-regulation of H3K4me3 and H3K9ac [54–56].

Increasing evidence suggests that virus infection can regulate histone modification [57–63]. BmNPV infections can up-regulate H3K4me2 and H3K4me3 in *B. mori* [59]. In this study, we report levels of H3K9me3 to be down-regulated 48 h post-infection with BmCPV and levels of H3K9me3 to be up-regulated at 96-h post-infection. However, the opposite occurs with H3K9ac levels, suggesting that regulation of

virus infection on H3K9me3 and H3K9ac is dynamic. H3K9me3 is mostly enriched in regions outside the gene and often co-located with retrotransposons [64]. However, H3K9me3 can also be enriched at intron and exon regions [65,66], and some promoters [67]. H3K9ac was mostly enriched downstream of TSS [68,69]. We report H3K9me3/H3K9ac-enriched peaks to occur mostly in distal intergenic regions, then promoter regions, introns and exons, and for BmCPV infection to have no significant effect on the distribution of H3K9me3/H3K9ac modifications. As a typical suppressive epigenetic marker, H3K9me3 is closely related to heterochromatin formation and transcriptional silencing [70–72]. H3K9me3 enriched in the gene body outside transcription initiation sites correlates positively with transcriptional activity, especially gene expression in the heterochromatin region [73,74]. However, H3K9ac, a typical active epigenetic marker, is closely related to transcription initiation and elongation [75]. We report H3K9ac modification to be associated with gene transcriptional activation, and for the effect of H3K9me3 on gene expression to depend on the H3K9me3 level and H3K9me3-enriched regions.

Responses of the host to infection vary depending on the virus, so changes in histone modifications after viral infection are specific. H3K9me3-enriched genes caused by EBV infection are mainly annotated in the neuron function and protein kinase A pathway, whereas levels of H3K9ac at sites of EBV nuclear antigens that are critical for lymphoblastoid cell line outgrowth increased [12,76]. Proteins encoded by HBV can promote enrichment of H3K9me3 in genes related to cell migration, DNA modification, and ARF protein signal transduction [77]. Severe acute respiratory syndrome coronavirus 2 infection led to the enrichment of H3K9me3 in genes related to protein glycosylation and glycan regulation [78]. In cells infected with HIV-1, the histone islands with reduced H3K9ac enrichment were annotated into a p63 transcription factor network, whereas

Scatter plots of the correlations between all CUT&Tag signals for H3K9ac and all gene expression levels in promoter regions. The X-axis represented CUT&Tag-seq signal levels for H3K9ac (\log_2 RPM of the promoter region), and the Y-axis represented gene expression levels(FPKM). The yellower the dot was, the stronger the relevance between gene expression level and CUT&Tag-seq in promoter was. Due to the presence of two biological replicates in each group, the average value of all replicates within that group was taken. (c) CUT&Tag signal distribution of genes from RNA-seq. Genes from RNA-seq were classified into one of five bins based on their FPKM values. The X-axis represented gene regions(from 3000 bp upstream of the TSS to 3000 bp downstream from the TESs) and the Y-axis represented average CUT&Tag signals for H3K9ac(RPM). TSS, transcription start sites; TES, transcription end sites. (d) Cumulative distribution function (CDF) plots and boxplots of three groups of genes. The genes were divided into up-, non- and down-regulated genes based on gene expression levels \log_2 foldchange. in CDF plots, the X-axis represented H3K9ac CUT&Tag-seq RPM values \log_2 foldchange of up-, non- and down-regulated genes while the Y-axis represented cumulative fraction values. In boxplots, the X-axis represented three groups of genes, including up-, non- and down-regulated genes and the Y-axis represented H3K9ac CUT&Tag-seq RPM values (\log_2 foldchange). *p* values were obtained by KS tests on CUT&Tag-seq RPM of three types of genes pairwise. (e) CDF plots of genes related to differential H3K9ac peaks. The X-axis represented RNA-seq FPKM \log_2 foldchange and the Y-axis represented cumulative fraction values. *p* values were obtained by KS tests on RNA-seq FPKM of three types of genes pairwise.

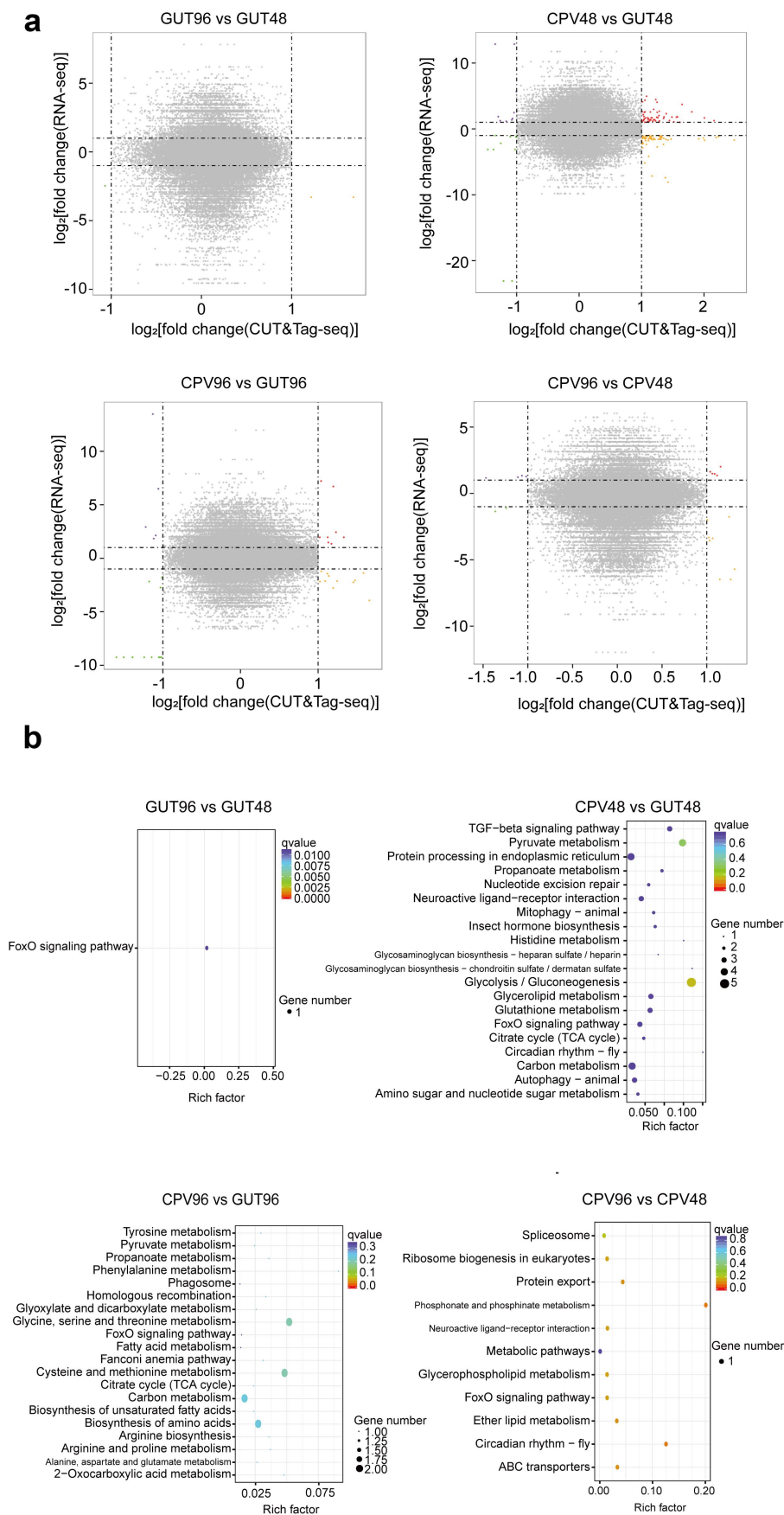


Figure 8. Identification of H3K9ac-related intersection genes. (a) Quadrantal distribution plots of H3K9ac-related and differentially expressed genes. The X-axis represented the RNA-seq FPKM log₂foldchange and the Y-axis represented CUT&Tag-seq of all H3K9ac

islands with increased H3K9ac enrichment were involved in the RNA polymerase III transcription termination pathway [79]. BoHV-1 infection can decrease H3K9ac enrichment in nuclear factor erythroid 2 p45-related factor 2 genes, which are a key transcriptional factor regulating a panel of antioxidant and cellular defence genes in response to oxidative stress [14]. Using GO enrichment analysis, we identify differential H3K9me3-enriched genes in cytoplasm and cellular component organization at 48 h post-infection and centromere regions and anatomical structure homeostasis at 96 h post-infection; and for differential H3K9ac-enriched genes to be assigned to mitochondrial outer membrane, and organelle outer membrane at 48 h post-infection, and linked to nucleoside-triphosphatase regulator activity, and small GTPase mediated signal transduction at 96 h post-infection. These results indicate that GO terms annotated with differential H3K9ac/H3K9me3 peak-related genes changed with BmCPV infection and that an association between H3K9ac/H3K9me3 modification and viral infection exists.

H3K4me3-enriched genes were annotated to the toll-like receptor pathway in zebrafish after infection with spring viraemia of carp virus [80]. We found differential H3K9me3-peak-related genes to be mainly enriched in the MAPK and Wnt signalling pathways at 48 h post-infection with BmCPV, and enriched in the MAPK and Hippo signalling pathways at 96 h post-infection. Differential H3K9ac-peak-related genes were mainly enriched in the Hippo signalling pathway and citrate cycle (TCA cycle) at 48 h post-infection, and neuroactive ligand-receptor interaction and dorso-ventral axis formation at 96 h post-infection. Differential H3K9me3- and H3K9ac-peak-related genes were both enriched in the Hippo signalling pathway, which plays a key role in controlling tissue size [81]. Silkworms infected with BmCPV are thin and small. Therefore, we speculate that the size of the infected silkworm body may be jointly regulated by H3K9me3 and H3K9ac.

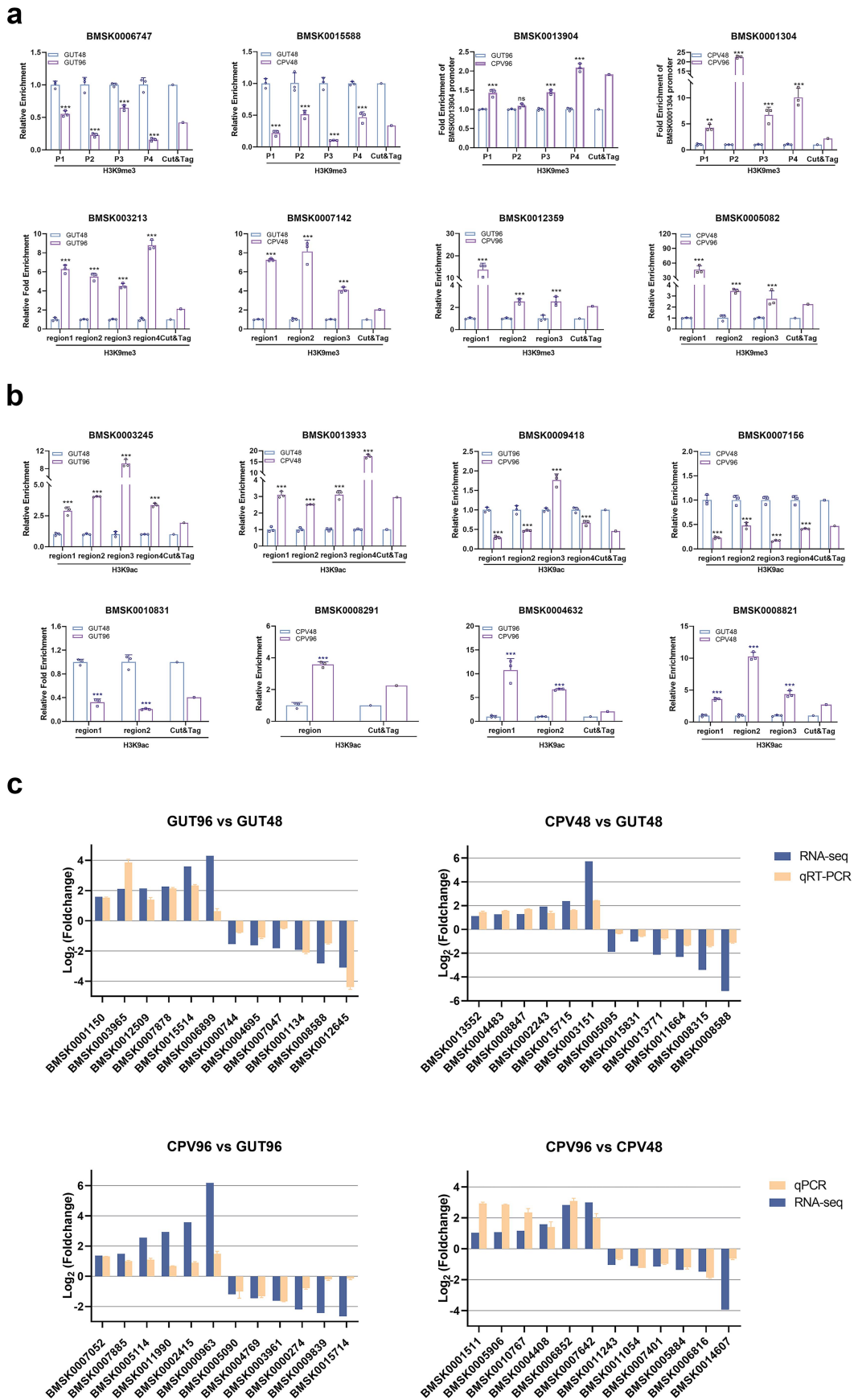
Gene expression profiles changed with *B. mori* latent virus (BmLV) [82], *B. mori* bidensovirus (BmBDV) [83], BmNPV [84] and BmCPV infection [85]. We report numbers of up-regulated genes to exceed those of down-regulated genes in the CPV48 vs GUT48 comparison. In the CPV96 vs GUT96 comparison, there were fewer up-regulated genes than down-regulated

genes. DEGs in the CPV48 vs GUT48 comparison were mainly enriched in transmembrane transport and transmembrane transporter activity GO terms at 48 h post-infection. DEGs in the CPV96 vs GUT96 comparison were enriched in oxidoreductase activity, acting on NAD(P)H, and mitochondrial inner membrane GO terms. Therefore, we infer that substance transport is mainly affected during the early stages of BmCPV infection and that energy metabolism is mainly affected in the later stages of BmCPV infection. KEGG enrichment analysis revealed DEGs to be mainly enriched in the synthesis of amino acids in the GUT96 vs GUT48 comparison, possibly because silk protein synthesis occurs during the development of the 5th instar silkworm. DEGs in the CPV48 vs GUT48 comparison were mainly enriched in carbon metabolism and glycolysis/gluconeogenesis pathway, while those in the CPV96 vs GUT96 comparison were mainly enriched in the oxidative phosphorylation pathway and pentose and glucuronate interconversions; this suggests that regulation of carbon metabolism occurs mainly during early BmCPV infection stages, and that of energy metabolism occurs in later infection stages.

In eukaryotes, the initial gene expression pattern at the whole genome level depends on chromatin accessibility [86,87]. H3K9me3 is closely related to gene transcript silencing [88,89], while H3K9ac is related to gene transcript activation [90]. Gene expression can be regulated by EBV, KSHV, and HBV infections at the whole genome level by changing histone modifications [18,19,70–72,77,91]. We report the modification levels of H3K9me3/H3K9ac to change significantly with BmCPV infection, and for the two to trend in opposite ways. This suggests a transition between H3K9me3 and H3K9ac, that is caused by histone methyltransferases and HATs. When histone methyltransferases are released from chromatin, the exposure of H3K9me3 occurs and allows the binding of HATs to H3K9, resulting in a transition of H3K9me3 to H3K9ac [92–94]. This transition is dynamic [95]. Changes in gene expression patterns at the whole genome level are related to the dynamic modification of histones after BmCPV infection.

We report a complex correlation between H3K9me3/H3K9ac mark and gene expressions, with integration analysis between CUT&Tag-seq peak signals and RNA-seq FPKM. Results indicate gene

peaks \log_2 foldchange. The dashed lines represented that the absolute value of RNA-seq FPKM \log_2 foldchange was 1 or the absolute value of CUT&Tag-seq of all H3K9ac peaks \log_2 foldchange was 1. (b) KEGG enrichment of intersection genes. The Y-axis represented the KEGG pathway, and the X-axis represented the rich factor. Qvalue, corrected *p*-value.



expression levels correlate negatively with the intensity of H3K9me3 peak signals in the gene body, and positively with the intensity of H3K9me3 peak signals in promoters. This suggests that the impact of H3K9me3 modification on gene expression depends on the region where the H3K9me3 modification is located, consistent with previous reports [70–72]. Gene expression levels correlate positively with the intensity of CUT&Tag-seq H3K9ac signals at TSS [96,97]. We report the effect of H3K9ac modification on gene expression levels with different RNA-seq (\log_2 foldchange) to differ after silkworms were infected with BmCPV, indicating that BmCPV infection altered the impact of H3K9ac modification on gene expression.

KEGG analysis revealed that the intersection genes with the \log_2 foldchange of both H3K9me3 peak and RNA-seq FPKM > 1 were enriched in insect hormone biosynthesis and the MAPK signalling pathway in the CPV48 vs GUT48 comparison, and oxidative phosphorylation, TGF-beta signalling pathway, insect hormone biosynthesis, and the MAPK signalling pathway in the CPV96 vs GUT96 comparison. MAPK cascades play key roles in proliferation, differentiation, apoptosis, and stress responses [98]. Intersection genes with \log_2 foldchange in both H3K9ac peak and RNA-seq FPKM > 1 were enriched into glycolysis/gluconeogenesis, pyruvate metabolism, TGF-beta signalling pathway, insect hormone biosynthesis, and mitophagy-animal in the CPV48 vs GUT48 comparison, and glycine, serine and threonine metabolism, cysteine and methionine metabolism, and biosynthesis of amino acids in the CPV96 vs GUT96 comparison. Activation of the MAPK signalling pathway is required for efficient infection by BmNPV [1]. Therefore, we suggest that the role of the MAPK signalling pathway in BmCPV infection is regulated by H3K9me3/H3K9ac modification. Autophagy, apoptosis, and growth and development of silkworm cells are regulated by insect hormones [99,100]. After being infected with BmCPV, silkworm development is hindered, leading to autophagy [101]. We speculate that BmCPV infection inhibits the development of silkworms by regulating H3K9me3/H3K9ac modification levels of genes related to insect hormone biosynthesis. BmCPV specifically

infects the silkworm midgut. We report DEGs regulated by H3K9ac to be enriched in glycolysis/gluconeogenesis, pyruvate metabolism, and amino acid metabolism, which may explain the small body of BmCPV-infected silkworms.

In conclusion, H3K9me3/H3K9ac and gene expression profiles at the genome-wide level changed with BmCPV infection, changes in gene expression profiles associated with H3K9me3/H3K9ac enrichments at gene regions occurred, a negative correlation existed between H3K9me3 enrichments at gene bodies and gene expression, and a positive correlation existed between H3K9ac enrichments at TSS. Intersection genes shared by differential H3K9me3 peak-related genes and DEGs were enriched in insect hormone biosynthesis, MAPK signalling, and TGF-beta signalling pathways, and genes shared by differential H3K9ac peak-related genes and DEGs were enriched in glycolysis/gluconeogenesis, and TGF-beta signalling and mitophagy pathways. These findings suggest that changes in gene expression levels caused by H3K9me3/H3K9ac modifications are associated with BmCPV infection in silkworms.

Disclosure statement

No potential conflict of interest was reported by the author(s).

Funding

This work was supported by the National Natural Science Foundation of China [32072792, 32372946 and 32202744], the National Key Research and Development Program of China [2019YFA0905200], Jiangsu Agricultural Science and Technology Innovation Fund (JASTIF) of China [CX (23) 1042], the Priority Academic Program of Development of Jiangsu Higher Education Institutions [YL13430023] and Suzhou Agricultural Science and Technology Innovation Project [grant no. SNG2021033].

Authors' contributions

The project was conceived and supervised by C.G. and X.H. And Q.Q., Z.L., H.P. and L.L. collected samples, finished the experiments, and organized the main text. Q.Q., X.T. and M. Z. conducted bioinformatic analyses, drafted the manuscript, and prepared the tables and figures. M.Z. and Y.F. guided the

small regions(about 250 bp per region). The CUT&Tag bar represented the average foldchange of differential H3K9me3/H3K9ac peak from CUT&Tag sequencing. The Y-axis represented the relative enrichment of the gene regions in two groups. (ns, $p > 0.05$; * $p < 0.05$; ** $p < 0.01$; *** $p < 0.001$). (a) Changes of H3K9me3 levels in gene regions. (b) Changes of H3K9me3 levels in gene regions. (c) Expression levels of DEGs. The expression levels of DEGs were detected by qPCR. The Y-axis represented foldchanges of DEGs in GUT96 vs GUT48, CPV48 vs GUT48, CPV96 vs GUT96 and CPV96 vs CPV48 group, respectively. The X-axis represented gene ID of DEGs confirmed by qPCR. Please note that foldchanges are expressed as \log_2 values (a 2-fold up- or down-regulation corresponds to a \log_2 value of 1 or – 1, respectively).

manuscript development and revision. All the authors participated in the drafting or revising of the manuscript and approved the final manuscript.

Availability of data and materials

The ChIP-qPCR and qPCR data supporting the findings of this study are openly accessible in the Science Data Bank at <https://doi.org/10.57760/sciencedb.17808>. The data except for ChIP-qPCR and qPCR data are shown in the Supplemental materials.

ORCID

Chengliang Gong  <http://orcid.org/0000-0001-6545-727X>

References

- [1] Katsuma S, Mita K, Shimada T. ERK- and JNK-Dependent signaling pathways contribute to Bombyx mori Nucleopolyhedrovirus infection. *J Virol*. 2007;81(24):13700–13709. doi: 10.1128/JVI.01683-07
- [2] Zhang Y, Sun Z, Jia J, et al. Overview of histone modification. *Adv Exp Med Biol*. 2021;1283:1–16.
- [3] Greer EL, Shi Y. Histone methylation: a dynamic mark in health, disease and inheritance. *Nat Rev Genet*. 2012;13(5):343–357. doi: 10.1038/nrg3173
- [4] Back F. The variable condition of euchromatin and heterochromatin. *Int Rev Cytol*. 1976;45:25–64.
- [5] Bannister AJ, Zegerman P, Partridge JF, et al. Selective recognition of methylated lysine 9 on histone H3 by the HP1 chromo domain. *Nature*. 2001;410(6824):120–124. doi: 10.1038/35065138
- [6] Matsui T, Leung D, Miyashita H, et al. Proviral silencing in embryonic stem cells requires the histone methyltransferase ESET (vol 464, pg 927, 2010). *Nature*. 2014;513(7516):128–128. doi: 10.1038/nature13610
- [7] Imai K, Kamio N, Cueno ME, et al. Role of the histone H 3 lysine 9 methyltransferase Suv39 h1 in maintaining Epstein-Barr virus latency in B 95-8 cells. *FEBS J*. 2014;281(9):2148–2158. doi: 10.1111/febs.12768
- [8] Lang FC, Li X, Vladimirova O, et al. CTCF interacts with the lytic HSV-1 genome to promote viral transcription. *Sci Rep-Uk*. 2017;7(1):7. doi: 10.1038/srep39861
- [9] Tsai MS, Chen SH, Chang CP, et al. Integrin-linked kinase reduces H3K9 Trimethylation to enhance herpes simplex virus 1 replication. *Front Cell Infect Microbiol*. 2022;12:12. doi: 10.3389/fcimb.2022.814307
- [10] Yuan PP, Yan J, Wang S, et al. Trim28 acts as restriction factor of prototype foamy virus replication by modulating H3K9me3 marks and destabilizing the viral transactivator tas. *Retrovirology*. 2021;18(1). doi: 10.1186/s12977-021-00584-y
- [11] Deutsch MJ, Ott E, Papior P, et al. The latent origin of replication of Epstein-Barr virus directs viral genomes to active regions of the nucleus. *J Virol*. 2010;84(5):2533–2546. doi: 10.1128/JVI.01909-09
- [12] Portal D, Zhou H, Zhao B, et al. Epstein-Barr virus nuclear antigen leader protein localizes to promoters and enhancers with cell transcription factors and EBNA2. *Proc Natl Acad Sci USA*. 2013;110(46):18537–18542. doi: 10.1073/pnas.1317608110
- [13] Bhattacharjee S, Bose P, Patel K, et al. Transcriptional and epigenetic modulation of autophagy promotes EBV oncoprotein EBNA3C induced B-cell survival. *Cell Death Dis*. 2018;9(6):605. doi: 10.1038/s41419-018-0668-9
- [14] Fu XT, Chen DM, Ma Y, et al. Bovine herpesvirus 1 productive infection led to inactivation of Nrf2 signaling through diverse approaches. *Oxid Med Cell Longev*. 2019;2019:1–14. doi: 10.1155/2019/4957878
- [15] Zhu L, Jiang X, Fu X, et al. The involvement of histone H3 acetylation in bovine herpesvirus 1 replication in MDBK cells. *Viruses*. 2018;10(10):525. doi: 10.3390/v10100525
- [16] Wei FF, Meng D. Study on the role of histone epigenetic modification in replication of hepatitis B virus. *Biochem Bioph Res Co*. 2023;669:1–9. doi: 10.1016/j.bbrc.2023.05.045
- [17] Yuan YF, Zhao KT, Yao YX, et al. HDAC11 restricts HBV replication through epigenetic repression of cccDNA transcription. *Antivir Res*. 2019;172:172. doi: 10.1016/j.antiviral.2019.104619
- [18] Mirzaei H, Ghorbani S, Khanizadeh S, et al. Histone deacetylases in virus-associated cancers. *Rev Med Virol*. 2020;30(1). doi: 10.1002/rmv.2085
- [19] Toth Z, Maglinte DT, Lee SH, et al. Epigenetic analysis of KSHV latent and lytic genomes. *PLOS Pathog*. 2010;6(7):e1001013. doi: 10.1371/journal.ppat.1001013
- [20] Cheng D, Cheng TC, Yang X, et al. The genome-wide transcriptional regulatory landscape of ecdysone in the silkworm. *Epigenet Chromatin*. 2018;11(1):11. doi: 10.1186/s13072-018-0216-y
- [21] Cheng D, Dong ZM, Lin P, et al. Transcriptional activation of ecdysone-responsive genes requires H3K27 acetylation at enhancers. *Int J Mol Sci*. 2022;23(18):10791. doi: 10.3390/ijms231810791
- [22] Xu GF, Lyu H, Yi YQ, et al. Intragenic DNA methylation regulates insect gene expression and reproduction through the MBD/Tip60 complex. *Iscience*. 2021;24(2):102040. doi: 10.1016/j.isci.2021.102040
- [23] Li ZQ, Mon H, Mitsunobu H, et al. Dynamics of polycomb proteins-mediated histone modifications during UV irradiation-induced DNA damage. *Insect Biochem Molec*. 2014;55:9–18. doi: 10.1016/j.ibmb.2014.10.001
- [24] Shoji K, Kokusho R, Kawamoto M, et al. H3K4me3 histone modification in baculovirus-infected silkworm cells. *Virus Genes*. 2021;57(5):459–463. doi: 10.1007/s11262-021-01858-5
- [25] Wu P, Wang X, Qin GX, et al. Microarray analysis of the gene expression profile in the midgut of silkworm infected with cytoplasmic polyhedrosis virus. *Mol Biol Rep*. 2011;38(1):333–341. doi: 10.1007/s11033-010-0112-4
- [26] Zhang ZD, Zhao Z, Lin S, et al. Identification of long noncoding RNAs in silkworm larvae infected with Bombyx mori cypovirus. *Arch Insect Biochem*. 2021;106(3):1–12. doi: 10.1002/arch.21777

- [27] Wu P, Han SH, Chen T, et al. Involvement of MicroRNAs in infection of silkworm with Cytoplasmic Polyhedrosis Virus (BmCPV). *PLOS ONE*. 2013;8(7): e68209. doi: [10.1371/journal.pone.0068209](https://doi.org/10.1371/journal.pone.0068209)
- [28] Hu XL, Zhu M, Zhang X, et al. Identification and characterization of circular RNAs in the silkworm midgut following *Bombyx mori* cytoplasmic polyhedrosis virus infection. *RNA Biol*. 2018;15(2):292–301. doi: [10.1080/15476286.2017.1411461](https://doi.org/10.1080/15476286.2017.1411461)
- [29] Gao K, Deng XY, Shang MK, et al. iTRAQ-based quantitative proteomic analysis of midgut in silkworm infected with cytoplasmic polyhedrosis virus. *J Proteomics*. 2017;152:300–311. doi: [10.1016/j.jprot.2016.11.019](https://doi.org/10.1016/j.jprot.2016.11.019)
- [30] Igolkina AA, Zinkevich A, Karandasheva KO, et al. H3K4me3, H3K9ac, H3K27ac, H3K27me3 and H3K9me3 histone tags suggest distinct regulatory evolution of open and condensed chromatin landmarks. *Cells-Basel*. 2019;8(9):1034. doi: [10.3390/cells8091034](https://doi.org/10.3390/cells8091034)
- [31] Nicetto D, Zaret KS. Role of H3K9me3 heterochromatin in cell identity establishment and maintenance. *Curr Opin Genet Dev*. 2019;55:1–10. doi: [10.1016/j.gde.2019.04.013](https://doi.org/10.1016/j.gde.2019.04.013)
- [32] Zhang YL, Cao GL, Zhu LY, et al. Integrin beta and receptor for activated protein kinase C are involved in the cell entry of cypovirus. *Appl Microbiol Biot*. 2017;101(9):3703–3716. doi: [10.1007/s00253-017-8158-z](https://doi.org/10.1007/s00253-017-8158-z)
- [33] Bartosovic M, Kabbe M, Castelo-Branco G. Single-cell CUT&Tag profiles histone modifications and transcription factors in complex tissues. *Nat Biotechnol*. 2021;39(7):825–835. doi: [10.1038/s41587-021-00869-9](https://doi.org/10.1038/s41587-021-00869-9)
- [34] Kaya-Okur HS, Wu SJ, Codomo CA, et al. CUT&Tag for efficient epigenomic profiling of small samples and single cells. *Nat Commun*. 2019;10(1):10. doi: [10.1038/s41467-019-09982-5](https://doi.org/10.1038/s41467-019-09982-5)
- [35] Buenostro JD, Wu BJ, Litzenburger UM, et al. Single-cell chromatin accessibility reveals principles of regulatory variation. *Nature*. 2015;523(7561):486–U264. doi: [10.1038/nature14590](https://doi.org/10.1038/nature14590)
- [36] Zhang H, He L, Cai L. Transcriptome sequencing: RNA-Seq. *Methods Mol Biol*. 2018;1754:15–27.
- [37] Heinz S, Benner C, Spann N, et al. Simple combinations of lineage-determining transcription factors prime-regulatory elements required for macrophage and B cell identities. *Mol Cell*. 2010;38(4):576–589. doi: [10.1016/j.molcel.2010.05.004](https://doi.org/10.1016/j.molcel.2010.05.004)
- [38] Ramírez F, Dündar F, Diehl S, et al. deepTools: a flexible platform for exploring deep-sequencing data. *Nucleic Acids Res*. 2014;42(W1):W187–W191. doi: [10.1093/nar/gku365](https://doi.org/10.1093/nar/gku365)
- [39] Yu GC, Wang LG, He QY. ChIPseeker: an R/Bioconductor package for ChIP peak annotation, comparison and visualization. *Bioinformatics*. 2015;31(14):2382–2383. doi: [10.1093/bioinformatics/btv145](https://doi.org/10.1093/bioinformatics/btv145)
- [40] Young MD, Wakefield MJ, Smyth GK, et al. Gene ontology analysis for RNA-seq: accounting for selection bias. *Genome Biol*. 2010;11(2). doi: [10.1186/gb-2010-11-2-r14](https://doi.org/10.1186/gb-2010-11-2-r14)
- [41] Kanehisa M, Araki M, Goto S, et al. KEGG for linking genomes to life and the environment. *Nucleic Acids Res*. 2008;36:D480–D484. doi: [10.1093/nar/gkm882](https://doi.org/10.1093/nar/gkm882)
- [42] Lai B, Lee JE, Jang Y, et al. MLL3/MLL4 are required for CBP/p300 binding on enhancers and super-enhancer formation in brown adipogenesis. *Nucleic Acids Res*. 2017;45(11):6388–6403. doi: [10.1093/nar/gkx234](https://doi.org/10.1093/nar/gkx234)
- [43] Huang H, Weng H, Sun W, et al. Recognition of RNA N(6)-methyladenosine by IGF2BP proteins enhances mRNA stability and translation. *Nat Cell Biol*. 2018;20(3):285–295. doi: [10.1038/s41556-018-0045-z](https://doi.org/10.1038/s41556-018-0045-z)
- [44] Sathish P, Withana N, Biswas M, et al. Transcriptome analysis reveals season-specific rbcS gene expression profiles in diploid perennial ryegrass (*Lolium perenne* L.). *Plant Biotechnol J*. 2007;5(1):146–161. doi: [10.1111/j.1467-7652.2006.00228.x](https://doi.org/10.1111/j.1467-7652.2006.00228.x)
- [45] Lee JM, Roche JR, Donaghy DJ, et al. Validation of reference genes for quantitative RT-PCR studies of gene expression in perennial ryegrass (*Lolium perenne* L.). *BMC Mol Biol*. 2010;11(1):8. doi: [10.1186/1471-2199-11-8](https://doi.org/10.1186/1471-2199-11-8)
- [46] Cassidy LD, Young ARJ, Young CNJ, et al. Temporal inhibition of autophagy reveals segmental reversal of ageing with increased cancer risk. *Nat Commun*. 2020;11(1):307. doi: [10.1038/s41467-019-14187-x](https://doi.org/10.1038/s41467-019-14187-x)
- [47] Kim TH, Dekker J. ChIP–quantitative Polymerase Chain Reaction (ChIP-qPCR). *Cold Spring Harb Protoc*. 2018;2018(5):pdb.prot082628. doi: [10.1101/pdb.prot082628](https://doi.org/10.1101/pdb.prot082628)
- [48] Livak KJ, Schmittgen TD. Analysis of relative gene expression data using real-time quantitative PCR and the 2– $\Delta\Delta$ CT method. *Methods*. 2001;25(4):402–408. doi: [10.1006/meth.2001.1262](https://doi.org/10.1006/meth.2001.1262)
- [49] Rogers S, Moore M. Studies of the mechanism of action of the Shope rabbit papilloma virus. I. Concerning the nature of the induction of arginase in the infected cells. *J Exp Med*. 1963;117(3):521–542. doi: [10.1084/jem.117.3.521](https://doi.org/10.1084/jem.117.3.521)
- [50] Chen YH, MacGregor JP, Goldstein DA, et al. Histone modifications in simian virus 40 and in nucleoprotein complexes containing supercoiled viral DNA. *J Virol*. 1979;30(1):218–224. doi: [10.1128/jvi.30.1.218-224.1979](https://doi.org/10.1128/jvi.30.1.218-224.1979)
- [51] de La Fuente C, Deng L, Santiago F, et al. Gene expression array of HTLV type 1-infected T cells: up-regulation of transcription factors and cell cycle genes. *AIDS Res Hum Retroviruses*. 2000;16(16):1695–1700. doi: [10.1089/08892220050193164](https://doi.org/10.1089/08892220050193164)
- [52] Fujikawa D, Nakagawa S, Hori M, et al. Polycomb-dependent epigenetic landscape in adult T-cell leukemia. *Blood*. 2016;127(14):1790–1802. doi: [10.1182/blood-2015-08-662593](https://doi.org/10.1182/blood-2015-08-662593)
- [53] Perez S, Kaspi A, Domovitz T, et al. Hepatitis C virus leaves an epigenetic signature post cure of infection by direct-acting antivirals. *PLOS Genet*. 2019;15(6): e1008181. doi: [10.1371/journal.pgen.1008181](https://doi.org/10.1371/journal.pgen.1008181)
- [54] Busam KJ, Pulitzer MP, Coit DC, et al. Reduced H3K27me3 expression in Merkel cell polyoma virus-positive tumors. *Mod Pathol*. 2017;30(6):877–883. doi: [10.1038/modpathol.2017.8](https://doi.org/10.1038/modpathol.2017.8)
- [55] McLaughlin-Drubin ME, Crum CP, Munger K. Human papillomavirus E7 oncoprotein induces KDM6A and KDM6B histone demethylase expression and causes epigenetic reprogramming. *Proc Natl Acad*

- Sci USA. 2011;108(5):2130–2135. doi: [10.1073/pnas.1009933108](https://doi.org/10.1073/pnas.1009933108)
- [56] Zhang Y, Dakic A, Chen R, et al. Direct HPV E6/Myx interactions induce histone modifications, pol II phosphorylation, and hTERT promoter activation. *Oncotarget*. 2017;8(56):96323–96339. doi: [10.18632/oncotarget.22036](https://doi.org/10.18632/oncotarget.22036)
- [57] Buschle A, Hammerschmidt W. Epigenetic lifestyle of Epstein-Barr virus. *Semin Immunopathol*. 2020;42(2):131–142. doi: [10.1007/s00281-020-00792-2](https://doi.org/10.1007/s00281-020-00792-2)
- [58] Ho JSY, Mok BW, Campisi L, et al. TOP1 inhibition therapy protects against SARS-CoV-2-induced lethal inflammation. *Cell*. 2021;184(10):2618–2632 e2617. doi: [10.1016/j.cell.2021.03.051](https://doi.org/10.1016/j.cell.2021.03.051)
- [59] Kawaoka S, Hara K, Shoji K, et al. The comprehensive epigenome map of piRNA clusters. *Nucleic Acids Res*. 2013;41(3):1581–1590. doi: [10.1093/nar/gks1275](https://doi.org/10.1093/nar/gks1275)
- [60] Leong MML, Cheung AKL, Dai W, et al. EBV infection is associated with histone bivalent switch modifications in squamous epithelial cells. *P Natl Acad Sci USA*. 2019;116(28):14144–14153. doi: [10.1073/pnas.1821752116](https://doi.org/10.1073/pnas.1821752116)
- [61] Mikkelsen TS, Ku M, Jaffe DB, et al. Genome-wide maps of chromatin state in pluripotent and lineage-committed cells. *Nature*. 2007;448(7153):553–560. doi: [10.1038/nature06008](https://doi.org/10.1038/nature06008)
- [62] Naipauer J, Rosario S, Gupta S, et al. PDGFRA defines the mesenchymal stem cell Kaposi's sarcoma progenitors by enabling KSHV oncogenesis in an angiogenic environment. *PLOS Pathog*. 2019;15(12):e1008221. doi: [10.1371/journal.ppat.1008221](https://doi.org/10.1371/journal.ppat.1008221)
- [63] Park IY, Sohn BH, Yu E, et al. Aberrant epigenetic modifications in hepatocarcinogenesis induced by hepatitis B virus X protein. *Gastroenterology*. 2007;132(4):1476–1494. doi: [10.1053/j.gastro.2007.01.034](https://doi.org/10.1053/j.gastro.2007.01.034)
- [64] Barral A, Pozo G, Ducrot L, et al. SETDB1/NSD-dependent H3K9me3/H3K36me3 dual heterochromatin maintains gene expression profiles by bookmarking poised enhancers. *Mol Cell*. 2022;82(4):816–832.e12. doi: [10.1016/j.molcel.2021.12.037](https://doi.org/10.1016/j.molcel.2021.12.037)
- [65] Hu S, Wang X, Wang T, et al. Differential enrichment of H3K9me3 in intrahepatic cholangiocarcinoma. *BMC Med Genomics*. 2022;15(1):185. doi: [10.1186/s12920-022-01338-1](https://doi.org/10.1186/s12920-022-01338-1)
- [66] Wang X, Guo H, Yu F, et al. Keratin5-cytoskeleton-BMP4 network regulates cell phenotype conversions during cardiac regeneration. *Exp Cell Res*. 2022;418(1):113272. doi: [10.1016/j.yexcr.2022.113272](https://doi.org/10.1016/j.yexcr.2022.113272)
- [67] Sui WG, He HY, Yan Q, et al. ChIP-seq analysis of histone H3K9 trimethylation in peripheral blood mononuclear cells of membranous nephropathy patients. *Braz J Med Biol Res*. 2014;47(1):42–49. doi: [10.1590/1414-431X20132809](https://doi.org/10.1590/1414-431X20132809)
- [68] Hu YF, Lai Y, Chen XS, et al. Distribution pattern of histone marks potentially determines their roles in transcription and RNA processing in rice. *J Plant Physiol*. 2020;249:249. doi: [10.1016/j.jplph.2020.153167](https://doi.org/10.1016/j.jplph.2020.153167)
- [69] Wang Z, Zang C, Rosenfeld JA, et al. Combinatorial patterns of histone acetylations and methylations in the human genome. *Nat Genet*. 2008;40(7):897–903. doi: [10.1038/ng.154](https://doi.org/10.1038/ng.154)
- [70] de Castro Ij, Budzak J, Di Giacinto ML, et al. Repo-Man/PP1 regulates heterochromatin formation in interphase. *Nat Commun*. 2017;8(1):14048. doi: [10.1038/ncomms14048](https://doi.org/10.1038/ncomms14048)
- [71] Elgin SCR, Reuter G. Position-effect variegation, heterochromatin formation, and gene silencing in. *Csh Perspect Biol*. 2013;5(8):a017780–a017780. doi: [10.1101/cshperspect.a017780](https://doi.org/10.1101/cshperspect.a017780)
- [72] Kumar A, Kono H. Heterochromatin protein 1 (HP1): interactions with itself and chromatin components. *Biophys Rev*. 2020;12(2):387–400. doi: [10.1007/s12551-020-00663-y](https://doi.org/10.1007/s12551-020-00663-y)
- [73] Ninova M, Godneeva B, Chen YA, et al. The SUMO ligase Su(var)2–10 controls hetero- and euchromatic gene expression via establishing H3K9 trimethylation and negative feedback regulation. *Mol Cell*. 2020;77(3):571–585 e574. doi: [10.1016/j.molcel.2019.09.033](https://doi.org/10.1016/j.molcel.2019.09.033)
- [74] Riddle NC, Minoda A, Kharchenko PV, et al. Plasticity in patterns of histone modifications and chromosomal proteins in Drosophila heterochromatin. *Genome Res*. 2011;21(2):147–163. doi: [10.1101/gr.110098.110](https://doi.org/10.1101/gr.110098.110)
- [75] Gates LA, Shi J, Rohira AD, et al. Acetylation on histone H3 lysine 9 mediates a switch from transcription initiation to elongation. *J Biol Chem*. 2017;292(35):14456–14472. doi: [10.1074/jbc.M117.802074](https://doi.org/10.1074/jbc.M117.802074)
- [76] Kim KD, Tanizawa H, De Leo A, et al. Epigenetic specifications of host chromosome docking sites for latent Epstein-Barr virus. *Nat Commun*. 2020;11(1):877. doi: [10.1038/s41467-019-14152-8](https://doi.org/10.1038/s41467-019-14152-8)
- [77] Wang DY, An SH, Liu L, et al. Hepatitis B virus X protein influences enrichment profiles of H3K9me3 on promoter regions in human hepatoma cell lines. *Oncotarget*. 2016;7(51):84883–84892. doi: [10.18632/oncotarget.12751](https://doi.org/10.18632/oncotarget.12751)
- [78] Zhang Q, Wadgaonkar P, Xu L, et al. Environmentally-induced mdig contributes to the severity of COVID-19 through fostering expression of SARS-CoV-2 receptor NRPs and glycan metabolism. *Theranostics*. 2021;11(16):7970–7983. doi: [10.7150/thno.62138](https://doi.org/10.7150/thno.62138)
- [79] Kim KC, Lee S, Son J, et al. Identification of novel genes associated with HIV-1 latency by analysis of histone modifications. *Hum Genomics*. 2017;11(1):9. doi: [10.1186/s40246-017-0105-7](https://doi.org/10.1186/s40246-017-0105-7)
- [80] Medina-Gali R, Belló-Pérez M, Martínez-López A, et al. Chromatin immunoprecipitation and high throughput sequencing of SVCV-infected zebrafish reveals novel epigenetic histone methylation patterns involved in antiviral immune response. *Fish Shellfish Immun*. 2018;82:514–521. doi: [10.1016/j.fsi.2018.08.056](https://doi.org/10.1016/j.fsi.2018.08.056)
- [81] Heallen T, Zhang M, Wang J, et al. Hippo pathway inhibits wnt signaling to restrain cardiomyocyte proliferation and heart size. *Science*. 2011;332(6028):458–461. doi: [10.1126/science.1199010](https://doi.org/10.1126/science.1199010)
- [82] Kolliopoulou A, Van Nieuwerburgh F, Stravopodis DJ, et al. Transcriptome analysis of Bombyx mori larval midgut during persistent and pathogenic cytoplasmic polyhedrosis virus infection. *PLOS ONE*. 2015;10(3):e0121447. doi: [10.1371/journal.pone.0121447](https://doi.org/10.1371/journal.pone.0121447)
- [83] Sun Q, Guo HZ, Xia QY, et al. Transcriptome analysis of the immune response of silkworm at the early stage of bidensovirus infection. *Dev Comp Immunol*. 2020;106:103601. doi: [10.1016/j.dci.2019.103601](https://doi.org/10.1016/j.dci.2019.103601)

- [84] Hao BF, Li CY, Amanze C, et al. Identification of endoplasmic-reticulum-associated proteins involved in Bombyx mori nucleopolyhedrovirus entry by RNA-seq analysis. *Arch Virol.* **2022**;167(4):1051–1059. doi: [10.1007/s00705-022-05397-8](https://doi.org/10.1007/s00705-022-05397-8)
- [85] Wu P, Jie WC, Shang Q, et al. DNA methylation in silkworm genome may provide insights into epigenetic regulation of response to cypovirus infection. *Sci Rep-Uk.* **2017**;7(1):7. doi: [10.1038/s41598-017-16357-7](https://doi.org/10.1038/s41598-017-16357-7)
- [86] Klein DC, Hainer SJ. Genomic methods in profiling DNA accessibility and factor localization. *Chromosome Res.* **2020**;28(1):69–85. doi: [10.1007/s10577-019-09619-9](https://doi.org/10.1007/s10577-019-09619-9)
- [87] Klemm SL, Shipony Z, Greenleaf WJ. Chromatin accessibility and the regulatory epigenome. *Nat Rev Genet.* **2019**;20(4):207–220. doi: [10.1038/s41576-018-0089-8](https://doi.org/10.1038/s41576-018-0089-8)
- [88] Okada M, Lee L, Maekawa R, et al. Epigenetic changes of the Cyp11a1 promoter region in granulosa cells undergoing luteinization during ovulation in female rats. *Endocrinology.* **2016**;157(9):3344–3354. doi: [10.1210/en.2016-1264](https://doi.org/10.1210/en.2016-1264)
- [89] Severson PL, Tokar EJ, Vrba L, et al. Coordinate H3K9 and DNA methylation silencing of ZNFs in toxicant-induced malignant transformation. *Epigenetics-U.S.* **2013**;8(10):1080–1088. doi: [10.4161/epi.25926](https://doi.org/10.4161/epi.25926)
- [90] Yang L, Yu Y, Tian G, et al. H3K9ac modification was involved in doxorubicin induced apoptosis by regulating Pik3ca transcription in H9C2 cells. *Life Sci.* **2021**;284:284. doi: [10.1016/j.lfs.2021.119107](https://doi.org/10.1016/j.lfs.2021.119107)
- [91] Okabe A, Funata S, Matsusaka K, et al. Regulation of tumour related genes by dynamic epigenetic alteration at enhancer regions in gastric epithelial cells infected by Epstein-Barr virus. *Sci Rep-Uk.* **2017**;7(1):7. doi: [10.1038/s41598-017-08370-7](https://doi.org/10.1038/s41598-017-08370-7)
- [92] Ayoub N, Jeyasekharan AD, Bernal JA, et al. HP1- β mobilization promotes chromatin changes that initiate the DNA damage response. *Nature.* **2008**;453(7195):682–686. doi: [10.1038/nature06875](https://doi.org/10.1038/nature06875)
- [93] Monte-Serrano E, Morejon-Garcia P, Campillo-Marcos I, et al. The pattern of histone H3 epigenetic posttranslational modifications is regulated by the VRK1 chromatin kinase. *Epigenetics Chromatin.* **2023**;16(1):18. doi: [10.1186/s13072-023-00494-7](https://doi.org/10.1186/s13072-023-00494-7)
- [94] Sun Y, Jiang X, Xu Y, et al. Histone H3 methylation links DNA damage detection to activation of the tumour suppressor Tip60. *Nat Cell Biol.* **2009**;11(11):1376–1382. doi: [10.1038/ncb1982](https://doi.org/10.1038/ncb1982)
- [95] Ehrenhofer-Murray AE. Chromatin dynamics at DNA replication, transcription and repair. *Eur J Biochem.* **2004**;271(12):2335–2349. doi: [10.1111/j.1432-1033.2004.04162.x](https://doi.org/10.1111/j.1432-1033.2004.04162.x)
- [96] Song J, Henry H, Tian L, et al. Drought-inducible changes in the histone modification H3K9ac are associated with drought-responsive gene expression in Brachypodium distachyon. *Plant Biol (Stuttg).* **2020**;22(3):433–440. doi: [10.1111/plb.13057](https://doi.org/10.1111/plb.13057)
- [97] Xue R, Guo R, Li Q, et al. Rice responds to Spodoptera frugiperda infestation via epigenetic regulation of H3K9ac in the jasmonic acid signaling and phenylpropanoid biosynthesis pathways. *Plant Cell Rep.* **2024**;43(3):78. doi: [10.1007/s00299-024-03160-8](https://doi.org/10.1007/s00299-024-03160-8)
- [98] Guo YJ, Pan WW, Liu SB, et al. ERK/MAPK signalling pathway and tumorigenesis. *Exp Ther Med.* **2020**;19(3):1997–2007. doi: [10.3892/etm.2020.8454](https://doi.org/10.3892/etm.2020.8454)
- [99] Lin LB, Li HQ, Zheng QZ, et al. Research progress on the regulation of autophagy and apoptosis in insects by sterol hormone 20-hydroxyecdysone. *Insects.* **2023**;14(11):871. doi: [10.3390/insects14110871](https://doi.org/10.3390/insects14110871)
- [100] Malhotra P, Basu S. The intricate role of ecdysis triggering hormone signaling in insect development and reproductive regulation. *Insects.* **2023**;14(8):711. doi: [10.3390/insects14080711](https://doi.org/10.3390/insects14080711)
- [101] Zhu M, Pan J, Zhang MT, et al. Bombyx mori cypovirus (BmCPV) induces PINK1-parkin mediated mitophagy via interaction of VP4 with host Tom40. *Dev Comp Immunol.* **2022**;126:126. doi: [10.1016/j.dci.2021.104244](https://doi.org/10.1016/j.dci.2021.104244)